AD-781 230

GRASS: A DIGITAL COMPUTER RAY TRACING AND TRANSMISSION-LOSS-PREDICTION SYSTEM. VOLUME I. OVERALL DESCRIPTION

John J. Cernyn

Naval Research Laboratory
Washington, D.C.

FR-7621

21 December 1973

DISTRIBUTED BY:

NTIS

National Technical Information Service
U. S. DEPARTMENT OF COMMERCE
5285 Port Royal Road, Springfield Va. 22151

SECURITY CLASSIFICATION OF THIS PAGE (When Data Entered)

REPORT DOCUMENTATION PAGE

READ INSTRUCTIONS BEFORE COMPLETING FORM

1. REPORT NUMBER
NRL Report 7621

2. GOVT ACCESSION NO.

3. RECIPIENT'S CATALOG NUMBER

4. TITLE (and Subtitle)
GRASS: A DIGITAL-COMPUTER RAY-TRACING AND TRANSMISSION-LOSS-PREDICTION SYSTEM, VOLUME 1--OVERALL DESCRIPTION

5. TYPE OF REPORT & PERIOD COVERED
One phase of a continuing NRL Problem.

6. PERFORMING ORG. REPORT NUMBER

7. AUTHOR(s)
John J. Cornyn

8. CONTRACT OR GRANT NUMBER(s)

9. PERFORMING ORGANIZATION NAME AND ADDRESS
Naval Research Laboratory
Washington, D.C. 20375

10. PROGRAM ELEMENT, PROJECT, TASK AREA & WORK UNIT NUMBERS
NRL Problem S01-64B
RF 52-552 405-6221

11. CONTROLLING OFFICE NAME AND ADDRESS
Department of the Navy
Office of Naval Research
Arlington, Va. 22217

12. REPORT DATE
December 21, 1973

13. NUMBER OF PAGES
75

14. MONITORING AGENCY NAME & ADDRESS(if different from Controlling Office)

15. SECURITY CLASS. (of this report)
Unclassified

15a. DECLASSIFICATION/DOWNGRADING SCHEDULE

16. DISTRIBUTION STATEMENT (of this Report)
Approved for public release; distribution unlimited.

17. DISTRIBUTION STATEMENT (of the abstract entered in Block 20, if different from Report)

18. SUPPLEMENTARY NOTES

Reproduced by
NATIONAL TECHNICAL
INFORMATION SERVICE
U S Department of Commerce
Springfield VA 22151

19. KEY WORDS (Continue on reverse side if necessary and identify by block number)

Sonar	Refraction	Ray acoustics
Germinating Ray-Acoustics Simulation System (GRASS)	Digital computers	Underwater sound
	Fortran	Wave equation
Ray tracing	CDC 3800	Sound speed
Transmission loss	Acoustics	Hyperbolic partial differential eq.

20. ABSTRACT (Continue on reverse side if necessary and identify by block number)

GRASS (Germinating Ray-Acoustics Simulation System) is a set of linked digital computer programs (Fortran), or modules. These modules: (1) convert salinity, temperature, and depth (STD) data to sound-speed profiles; (2) interpolate and extrapolate the sound-speed field; (3) generate Calcomp or Gerber plots of the sound-speed profiles; (4) generate contour and three-dimensional isometric plots of the sound-speed field; (5) trace rays and calculate intensities; (6) generate ray diagrams; and (7) construct plots of the calculated transmission loss versus range. The system can handle multiple profiles

DD FORM 1 JAN 73 1473 EDITION OF 1 NOV 65 IS OBSOLETE
S/N 0102-014-6601

SECURITY CLASSIFICATION OF THIS PAGE (When Data Entered)

19. Continued

Eikonal equation
Geometrical acoustics
Long range underwater sound propagation
Deep ocean
Propagation
Wave theory
Normal mode theory
Caustics
Diffraction
Spreading loss
Inhomogeneous media
Geometrical optics
Multiple velocity profiles
Curvilinear profile
Linear segmented bottom
Calcomp plotting
Isometric plotting
Contour plotting
Computer applications—ray tracing

20. Continued

and a linear-segmented bottom profile. It is presently running on a CDC 3800. This report, the first of a two-volume set, includes an overview of each module, outlines the methods used in the calculations, provides the results of some test cases, makes some recommendations for improvement, and briefly compares ray and normal-mode theories.

PREFACE

This is the first of a two-volume set of reports describing a modular underwater acoustics ray-tracing and transmission-loss prediction system called GRASS (Germinating Ray-Acoustics Simulation System). This system is called "germinating" because, although it is presently operational, it could grow into a more powerful system.

The first volume is intended for the reader who is interested in gaining an overview of the system. It includes the theory behind each of the seven system modules, some of the guiding philosphy and techniques used in their implementation, qualitative comparisons with other ray-tracing and normal-mode approaches, the results of some sample test cases, and some recommendations for improvement.

The second volume (cited on the inside front cover) is intended for those who wish to use the system, or to compare it quantitatively with other ray acoustic systems. It describes in detail how to use the programs, and it contains a sample test case. The input data for this test case were obtained from experimental measurement. In addition, experimental transmission loss measurements were obtained and are given so that direct comparison can be made between computed and predicted results.

ACKNOWLEGMENTS

I thank the many individuals both within and without NRL who provided assistance and encouragement during the evolution of GRASS and the writing of this report. In particular, I thank Dr. Homer P. Bucker, former head of the Propagation Branch of the Acoustics Division of NRL, and Burton G. Hurdle, current head of the Propagation Branch, for their guidance and support, and Dr. Samuel W. Marshall and John Cybulski for reviewing the manuscript and offering many helpful suggestions.

CONTENTS

Preface iii

1. INTRODUCTION 1

1.1 Comparison of Ray Theory and Normal-Mode Theory.. 1
1.2 Computer Implementation of GRASS 4
1.3 Comparison of GRASS and Some Other Ray-Tracing Programs 7

2. MODELING THE OCEAN ENVIRONMENT 12

2.1 Treatment of the Sound-Speed Field 12

2.1.1 Conversion of Depth, Temperature, and Salinity Data to Sound-Speed Profiles (DTSTOV Program) 12
2.1.1.1 Purpose 12
2.1.1.2 Input 13
2.1.1.3 Output 13
2.1.1.4 Accuracy 13
2.1.1.5 Recommendations for Improvement . 14

2.1.2 Interpolation and Extrapolation of the Sound-Speed Field (VFC Program) 14
2.1.2.1 Purpose 14
2.1.2.2 Input 15
2.1.2.3 Output 15
2.1.2.4 Interpolation in Depth 15
2.1.2.5 Interpolation in Range 18
2.1.2.6 Earth-Curvature Correction 19
2.1.2.7 Algorithm 22
2.1.2.8 Sinusoidal-Profile Test Case 25
2.1.2.9 Recommendations for Improvement . 27

2.1.3 Profile Plotting (PRFPLT Program) 28
2.1.3.1 Purpose 28
2.1.3.2 Input 28
2.1.3.3 Output 28

2.1.4 Contouring and Generating Three-Dimensional Isometric Plots of the Sound-Speed Field (CTOUR Program) 30
2.1.4.1 Purpose 30
2.1.4.2 Input 30
2.1.4.3 Output 30
2.1.4.4 Algorithm 30
2.1.4.5 Test Methods and Results 31
2.1.4.6 Recommendations for Improvement . 31

2.2 Treatment of the Ocean Bottom 31
2.2.1 Representing the Bottom Topography 31
2.2.2 Describing the Bottom Losses 31

2.3 Treatment of the Ocean Surface 33
2.3.1 Describing the Surface 33
2.3.2 Describing the Surface Losses 33

2.4 Treatment of Attenuation 33

3. MODELING THE PROPAGATION OF SOUND 34

3.1 Ray Tracing and Intensity Calculations (SERPENT Program) 34
3.1.1 Purpose 34
3.1.2 Input 34
3.1.2.1 Punched Cards 34
3.1.2.2 Magnetic Tape 35

3.1.3 Output 35
3.1.3.1 Ray-Statistics Magnetic Tape (Optional) 35
3.1.3.2 Transmission-Loss Magnetic Tape (Optional) 36
3.1.3.3 Printer Listings (Optional) 36

3.1.4 Ray-Tracing Theory 37
3.1.4.1 Derivation of the Iteration Algorithm 37
3.1.4.2 Accuracy and Iterative Controls 42
3.1.4.3 An Example of the Order of Tracing All Rays Together in Range Segments 43
3.1.4.4 Error Analysis 44

3.1.5 Theory of Intensity Calculations 44
3.1.5.1 Describing the Source 44
3.1.5.2 Random Summation 44
3.1.5.3 Coherent Summation 48
3.1.5.4 Statistical Summation 48

3.1.6 Test Methods and Results 50
3.1.6.1 Untilted and Tilted Hyperbolic-Cosine Profiles 50
3.1.6.2 Gulf Stream Profiles 53

3.1.7 Recommendations for Improvement 53

3.2 Generating Ray Diagrams (RAPLOT Program) 58

3.2.1 Purpose 58
3.2.2 Input 58
3.2.3 Output 58
3.2.4 Recommendation for Improvement 58

3.3 Generating Transmission-Loss Plots (LOSSPLT Program) 58
3.3.1 Purpose 58
3.3.2 Input 58
3.3.3 Output 59

4. CONCLUSIONS AND RECOMMENDATIONS 59

REFERENCES 59

APPENDIX Basic Ray-Acoustics Theory 64

GRASS: A DIGITAL-COMPUTER RAY-TRACING AND TRANSMISSION-LOSS-PREDICTION SYSTEM, VOLUME 1—OVERALL DESCRIPTION

1. INTRODUCTION

1.1 Comparison of Ray Theory and Normal-Mode Theory

To a good first approximation, sound propagates in the ocean according to a linear hyperbolic second-order time-dependent partial differential equation, commonly referred to as the scalar wave equation:

$$\nabla^2\Phi = \frac{1}{c^2}\,\frac{\partial^2\Phi}{\partial t^2}\ . \tag{1}$$

In this equation ∇^2 is the Laplacian operator, c is the speed of sound, and Φ is either the acoustic pressure, the density perturbation, the particle velocity, or the scalar velocity potential. Eq. (1) follows directly from the equations of continuity, state, and motion [1]. This first approximation assumes only linear terms are kept, the condensation is small compared to unity, only irrotational motion is considered, and the derivative of pressure with respect to density is a constant. Throughout this report we will also assume that c is space dependent but time independent.

Usually the wave equation is solved to varying degrees of approximation by either ray or wave (normal-mode) theory. In reality the ray approach is an approximation of the wave approach. Here we are primarily concerned with the computer implementation of a ray theoretical approach. Frequently the normal-mode approach solves Eq. (1) by assuming a set of source and boundary conditions and applying standard techniques, such as those of Ref. 2. The ray theory approach, on the other hand, assumes a particular functional form for Φ to obtain another differential equation which is somewhat more amenable to solution. This new differential equation is commonly referred to as the eikonal equation. The Appendix discusses the eikonal equation and other fundamentals of ray acoustics in more detail.

Ray theory has the following advantages:

- It is versatile enough to handle highly variable bathymetry and complex depth- and range-dependent sound-speed fields.

- It provides a quantitative and easily visualized description of the propagation of sound in the form of ray diagrams.

- It is relatively straightforward and its equations are more tractable than those of normal-mode theory.

Manuscript submitted June 8, 1973.

- It fairly easily handles directive sources and receivers as well as pulsed sources.

Some of the disadvantages of ray theory are the following:

- In general, unmodified ray theory does not compare well with experiment at very low frequencies. One often quoted rule of thumb [3] is that ray theory is more "appropriate" than normal-mode theory provided

$$\lambda < \frac{h}{10}, \tag{2}$$

where h is the water depth and λ is the wavelength. Thus according to this rule a lower frequency limit for ray theory is approximately given by

$$f \approx \frac{10c}{h}. \tag{3}$$

If we set h to 3000 meters and c to 1500 meters/second, Eq. (3) gives a lower limit of approximately 5 Hz. Continuing with rules of thumb, the following statement by Williams [4] seems applicable:

> "For the ray approach to be safe the acoustic wavelength must be much smaller than any other pertinent length. 'Pertinent' lengths include the water depth, the size of obstacles, scale of surface and bottom roughness, distance in which the refractive index changes appreciably, and the size of any predicted focal region. It follows that at low acoustic frequencies any result of a ray calculation is suspect, although by no means necessarily wrong. *No exact figure for the onset of suspicion can be given; it depends upon the problem being tackled.* Examination of theoretical and experimental results suggests that, in the deep ocean, calculations at some 200 Hz and lower warrant examination by wave-acoustic theory; above some 1000 Hz, ray methods would usually be safe; in the interval, intercomparisons are desirable. Problems involving shallow-water regions, or shallow 'surface based ducts,' may require wave acoustic analysis at frequencies well above 200 Hz."

Substantiating the sentence italicized, comparison with experimental data using GRASS and other programs at NRL indicates that though there is certainly a lower limit to the frequencies amenable to ray-tracing techniques, even in the deep ocean, ray theory frequently gives good results at 100 Hz and at times is useful at frequencies as low as 50 Hz. Ray-tracing programs such as GRASS need not be strictly limited by all of the disadvantages of unmodified ray theory discussed above. For example, several methods have been proposed to more or less combine ray and wave theory and thereby correct intensities for the diffraction effects in the vicinity of caustics [5-11]. These and similar hybrid approaches will no doubt in the future extend the lower frequency limit and usefulness of ray-tracing programs. At present GRASS does not attempt to correct intensities for diffraction effects in the vicinity of caustics, although it could (and probably should) be modified to do so. It does however generate frequency dependent transmission-loss curves,

but only by using frequency dependent volume attenuation parameters, bottom loss tables, and source and receiver directivity functions.

- Prior to actually carrying out the ray calculations, one does not know exactly how many rays should be traced, at what angles, or even the angular spacing that should be used to achieve a certain degree of accuracy in the transmission-loss calculations.

- Usually in carrying out transmission-loss calculations many more rays are traced than are actually required. That is, only a small percentage of the rays traced will contribute significantly to the intensity at a particular receiver location.

Some of the advantages of normal mode theory are:

- It does not predict, as does unmodified ray theory, physically unrealistic false caustics and sharp shadow-zone boundaries.

- Its predictions are frequency dependent, in contrast to the frequency independent predictions of ray theory.

- It is valid over a much larger frequency range than ray theory.

- Its predictions, where computationally possible, tend to give better agreement with experimental data than those of ray theory.

- If only a few modes are excited, it tends to be more appropriate computationally than ray theory. For example, at very long ranges waveguide effects tend to dominate the propagation.

Some of the disadvantages of normal-mode theory are:

- In most cases involving initial and boundary conditions resembling those actually met in the ocean, the normal-mode calculation is at best laborious and at worst impossible.

- Existing normal-mode programs and solutions assume an elementary form of the bottom topography; indeed most solutions and programs mentioned in the literature assume a flat ocean bottom. Experimental evidence indicates however that the shape of the bottom can play a prominent role in propagation [12a].

- In normal-mode summations it is not always obvious how many modes (10 or 100?) should be included to obtain meaningful results.

- Normal-mode calculations generally require extreme accuracy in the calculation of mode contributions to obtain moderately accurate results [13]. Computer roundoff errors are a significant problem.

- It is more difficult for the average person to achieve an intuitive feel for the propagation of sound by examining normal-mode plots than by examining ray diagrams.

- For short ranges, wherein many modes are excited, ray theory solutions tend to be more practical from a computational standpoint than normal-mode solutions [14]. Normal-mode solutions involve a summation over continuous and discrete modes [15]. For long ranges and shallow water the discrete modes generally dominate; so most

solutions neglect the contribution from the continuous modes. For short ranges however the continuous modes dominate and the calculation of their contribution is difficult.

- The author knows of no normal-mode program which can handle multiple profiles and a variable bottom topography. The multiple-profile capability is of considerable importance, because it has been demonstrated both theoretically and experimentally that horizontal gradients are significant in long-range propagation [12a].

In summary, comparing the advantages and disadvantages of both ray and normal-mode theory, we see that from a theoretical point of view normal-mode theory has a significant number of advantages over ray theory. Unfortunately for our application the advantages of normal-mode theory are at present overshadowed by its computational disadvantages. For this reason we use the ray theory; the computational advantages and disadvantages tend to take precedence. But as advances continue to be made in computer science and numerical analysis, the computational difficulties posed by normal-mode theory will probably be overcome, and eventually it may replace ray theory, especially in the domain of low frequencies and long ranges.

1.2 Computer Implementation of GRASS

GRASS, Germinating Ray-Acoustics Simulation System, is a set of linked computer programs which comprises a ray-tracing and transmission-loss-prediction system. This system was designed primarily for studying the propagation of low-frequency sound over long ranges in the deep ocean. Because the ray-tracing technique described herein is based on, but not limited by, geometrical optics, the system could probably be adapted to many of the fields concerned with the propagation of waves in inhomogeneous media. For example, it could be modified for studying the propagation of acoustic waves in the atmosphere, of radio waves in the ionosphere, or light through a medium having a widely varying index of refraction [15-17].

The starting point in the development of this system was the Hudson Laboratories Ray-Tracing Program, HLRTP [12b]. Unfortunately, the majority of the HLRTP was written in a two-dimensional higher level computer language, USER [18-20], whose only compiler was located at the Hudson Laboratories. Rather than attempt to write a USER compiler for the NRL computer, a CDC 3800, we chose to start from the basic formulas contained in the HLRTP, to reanalyze and reformulate them, and to construct a completely new set of programs in the relatively universally understood higher level computer language Fortran. Since this new system is written in Fortran [21], it should be readily adaptable to most medium- and large-scale computer systems. The largest program requires 36,800 words of core (exclusive of CDC system routines).

GRASS bears only a slight resemblance to the HLRTP. Many of the algorithms and equations used in the HLRTP were initially adopted and modified, and some were eventually discarded. The resulting algorithms differ significantly from those in the HLRTP.

Figure 1 shows the present state of GRASS. The overall system is modular and contains seven program modules. Each module communicates with its neighboring programs via cards, or magnetic tape. This type of structure has several advantages over a single program that "does everything." Individual modules are easier to write, understand,

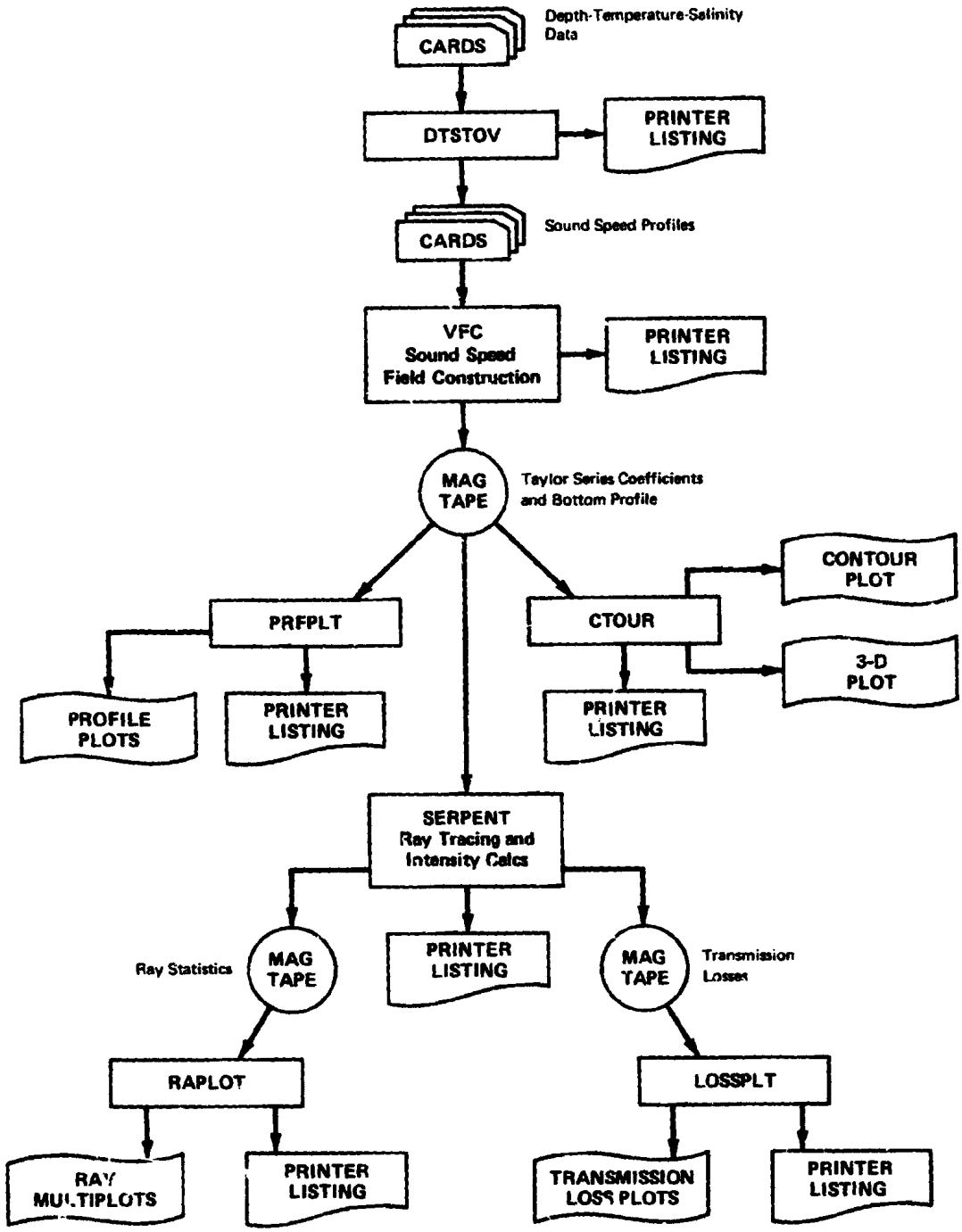

Fig. 1—GRASS System

modify, and document. In addition each module is easily adapted to several applications, whereas a "do everything" program would probably contain many irrelevant and core-consumming routines. Since each program has sole use of the computer's

memory while in execution, many of the difficulties experienced in writing large programs are avoided, such as having to overlay core. Further, the modular structure allows for uninhibited growth. As new ideas, experimental evidence, and applications arise, the existing programs can be revised and new programs linked into the system.

Briefly the seven modules (programs) shown in Fig. 1 perform the following functions:

Program	Function
DTSTOV	Converts depth, temperature, and salinity data to sound-speed profiles.
VFC	Interpolates and extrapolates the sound-speed field.
PRFPLT	Generates sound-speed, sound-speed-gradient, and sound-speed-curvature profile plots.
CTOUR	Generates a contour plot and three-dimensional isometric plot of the sound-speed field.
SERPENT	Carries out ray-tracing and transmission-loss computations.
RAPLOT	Generates ray diagrams.
LOSSPLT	Generates transmission-loss plots.

All of the above modules are stored in binary object form on a CDC 813 disk to allow for easy access by NRL scientists. The entire system requires approximately 55,000 (decimal) words of disk storage.

Some of the input features of GRASS are the following:

- It can handle a two-dimensional range- and depth-dependent sound-speed field.
- It can handle sound-speed profiles having up to 1000 points. There is no limit to the number of input profiles, and there are no restrictions on the spacings of profile-point depths.
- It permits the user to specify several bottom-loss tables and to indicate the ranges over which each of these tables applies.
- It has a free-field input routine for easy entry of data.
- It checks all data for proper entry and physical meaningfulness.
- It enables the user to insert a surface-loss parameter.
- It allows the user to specify simple beam patterns at the ray source.

Computational features of GRASS include the following:

- It uses multiple profiles having continuous first and second derivatives of sound speed with respect to depth and a discontinuous first derivative of sound speed with respect to range (if there are more than two input profiles).

- It allows the user to make tradeoffs between accuracy and running time.

- It traces up to 1500 rays concurrently in one pass through the sound-speed field.

- It extends both "shallow" and "deep" profiles to the ocean bottom. (These terms will be discussed later.)

- It corrects the sound-speed profiles, bottom topography, and source and receiver depths for earth curvature, if requested.

- It uses very elementary coherent- and random-phase intensity calculations for short ranges.

- It uses a statistical intensity calculation [12c] for intermediate and long ranges.

- It uses iterative rather than closed-form solutions to the ray equations.

Output characteristics of GRASS include the following:

- It produces Calcomp plots and printer listings which may be used directly in reports.

- It prints out complete ray statistics at ranges selected by the user.

- It generates three-dimensional plots and contour maps of the sound-speed field.

- It allows the user to generate ray diagrams directly from the ray tape. The user may select the rays he wishes to plot.

- It enables the user to plot transmission-loss and reference and/or experimental curves for multiple receiver depths on the same plot for comparison.

1.3 Comparison of GRASS and some Other Ray-Tracing Programs

Over most of the world's oceans the horizontal dependence of the sound-speed field is small compared to the depth dependence, but it is also true that for long-range propagation studies, of the distance of 100 miles or more, horizontal gradients cannot always be ignored [12d, 22]. Further, in some areas of the ocean the temperature gradients are so large that even for short ranges one cannot ignore horizontal gradients. An example of this phenomenon occurs in the vicinity of the Gulf Stream's circulating eddies [23] (Figs. 2 and 3). In these regions the ray patterns obtained by horizontal-gradient programs differ significantly from those obtained by programs which assume only a depth-dependent sound-speed field. Experience with GRASS has shown that horizontal gradients can move the sound channels up and down with respect to depth and also expand

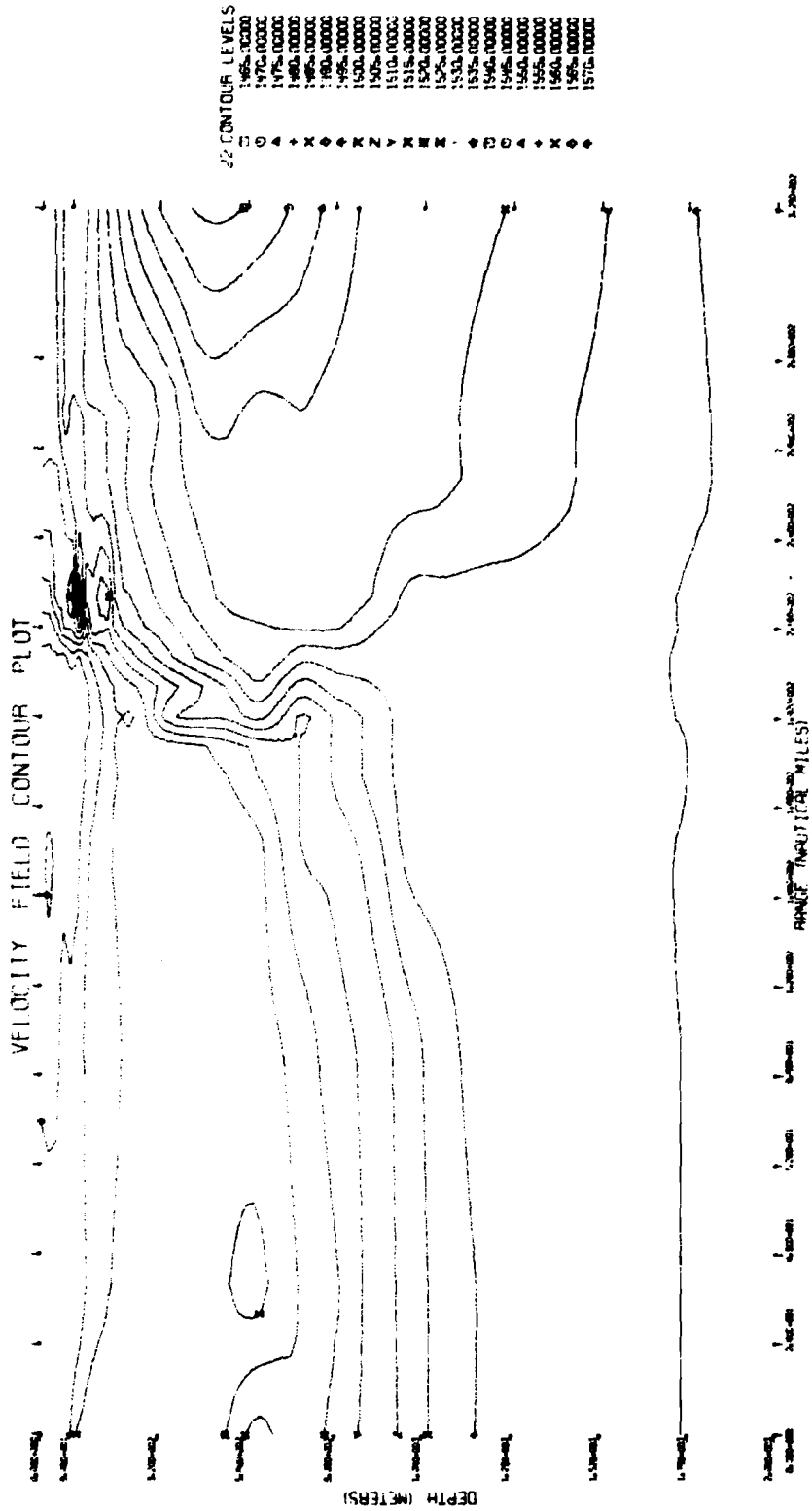

Fig. 2—Contour plot of the sound-speed field for the Gulf Stream in a test case

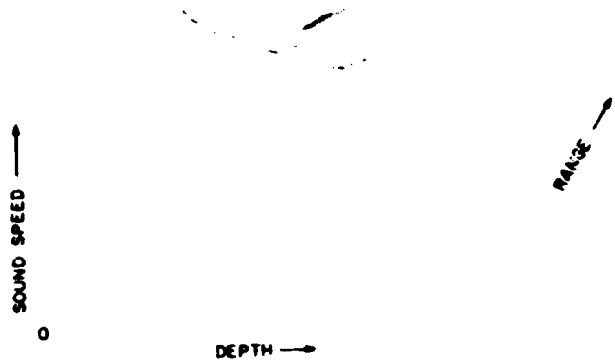

Fig. 3—Three-dimensional plot of the sound speed field for the Gulf Stream in the test case of Fig. 2

and contract them. Figure 4, generated by GRASS for the sound-speed field shown in Figs. 2 and 3, illustrates this behavior. These effects cannot be predicted by programs which use only a single profile to represent the sound-speed field. The reader may wish to examine the reports of Murphy and Lord [24] and Anderson [25] for some experimental measurements and further discussion of horizontal gradients. Warfield and Jacobson [26] show that even a weak range gradient can have a significant effect on pressure amplitudes and phase. Milder [27] discusses the relation of horizontal gradients to certain ray invariants.

Although there are a few notable exceptions [5, 16, 28-29], many of the ray-tracing programs available today cannot handle a range-dependent sound-speed field. That is, they assume the sound-speed field has only a depth dependence. Those which provide for only a depth-dependent sound-speed field give misleading results in numerous cases. For example some programs model the sound-speed field with a profile having discontinuous first and/or second derivatives of the sound speed with respect to depth. Discontinuities in the first derivative have been shown [30, 31] to lead to unrealistic regions of low intensity, spurious (false) caustics, and the omission of real caustics. Discontinuities in the second derivative can lead to layering effects in the form of infinite rates of change in intensity [32, 33].

Many ray-tracing programs place relatively severe limitations on the number of points a sound-speed profile may have. For example some programs provide for less than 50 points.

GRASS avoids these problems by using a representation of the sound-speed field having continuous first and second derivatives with respect to depth and taking into account horizontal gradients.

The GRASS ray-tracing program SERPENT achieves computational speed and efficiency by using iteration equations which allow for large increments in ray length; these iteration step sizes can approach 1000 meters and still give meaningful results. These large step sizes are motivated by the fact that in actual calculations the rays spend most of their time in the deeper regions of the ocean where the vertical gradients are small and

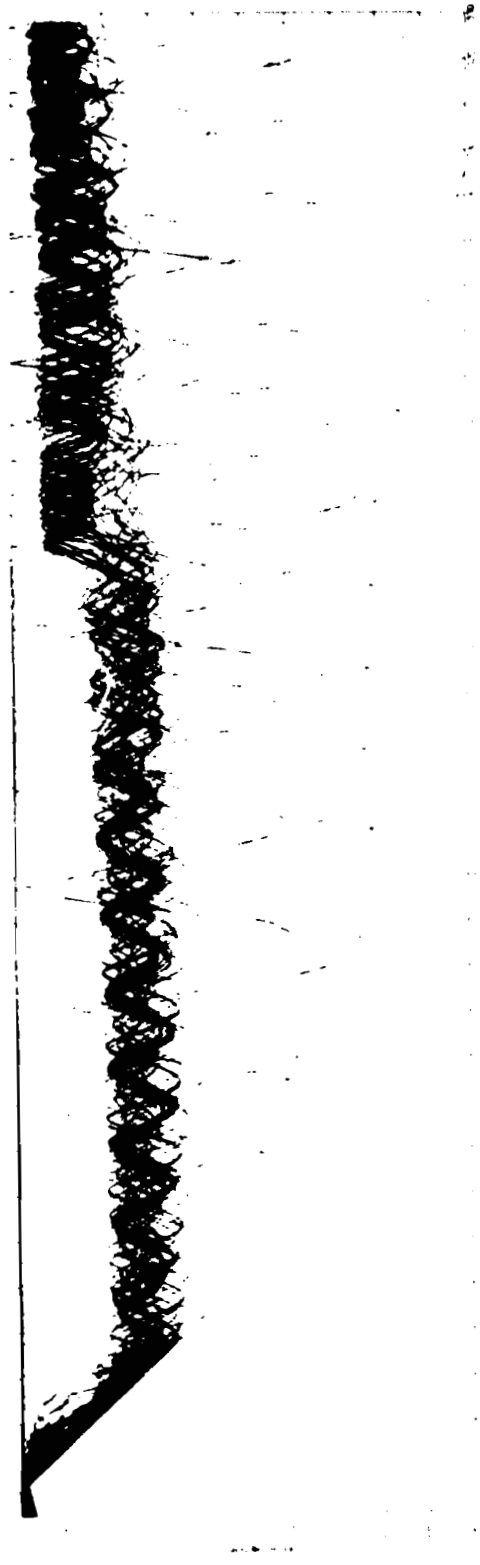

Fig. 4—Ray trace for the Gulf Stream in the test case Figs. 2 and 3. (In this figure the depth axis is expanded by a factor of about 34 relative to the range axis.)

nearly constant. As SERPENT traces a ray, it automatically adapts the ray's iteration step size to the local sound-speed field, contracts the ray arc increment in regions of high profile curvature and near turning points, and insures that the iterations do not pass too rapidly over the intervening profile structure. These procedures complement those contained in the VFC program of GRASS which detect and print warning messages for unusually large gradients and curvatures. In addition these adaptive procedures may be controlled by the user, allowing him to make a tradeoff between computation time and accuracy.

Further distinguishing GRASS from other ray-tracing programs is a procedure for estimating whether continued tracing of a ray is cost effective. Experience with GRASS has shown that the rays which are both most expensive to trace, in terms of computer time, and most difficult to trace, from a mathematical point of view, are also the ones that contribute least to the intensity at a distant receiver. For example the rays which leave the source at steep angles experience considerably more bottom hits than those leaving the source at near horizontal angles, and as a result their loss is also greater. Similarly it is quite common for rays to be trapped in very shallow surface ducts and undergo numerous surface hits within the distance of a few nautical miles. These same rays are ones for which ray theory may not be valid, as explained earlier. SERPENT constantly checks the rays as they are being traced to see that they are cost effective. If not, these rays are terminated, and the program goes on tracing more promising rays.

The GRASS ray-tracing technique uses an iterative rather than a closed-form solution to obtain ray paths. Some closed-form solutions are more desirable than some iterative solutions in that they are numerically stable and more conducive to analytic investigation [31a]. Nevertheless, closed-form solutions are not completely free of difficulties [34], and there are a number of advantages to an iterative approach. For example some closed-form solutions cannot be quickly evaluated on a computer, since they may require the evaluation of relations containing logarithmic, hyperbolic, and even more complicated functions. Furthermore a closed-form solution must represent the sound-speed field in a manner that adequately describes the actual physical phenomena, hence must avoid the discontinuity problems mentioned earlier and allow for horizontal gradients. A curve-fitting technique for obtaining a representation of the sound-speed field from oceanographic data should be straightforward and easily implemented on a computer. In addition, a closed-form solution should not restrict the shape of the bottom topography or the ray angles that can be traced. For example, because they are limited to certain closed-form solutions, some ray-tracing programs have difficulty accurately tracing near-horizontal rays.

Finally some ray-tracing programs [28] use a triangular-region representation of the sound-speed field. This representation forces the bottom profile to be linearly segmented. In SERPENT this problem does not arise. The ray-tracing equations are completely independent of the shape of the bottom profile and vice versa. There is no reason a curvilinear bottom, represented by a cubic spline, could not be incorporated into SERPENT, and there would be an advantage in using a representation of the bottom profile having continuous derivatives. In particular, since rays define a wavefront which physically must be continuous and smooth, adjacent rays which reflect from different bottom segments cannot represent physical reality.

A closed-form solution satisfying all of the desirable criteria mentioned is not easily obtained. Of course, all so-called closed-form solutions, once put on a computer, are

reduced to numerical approximations. Hence the problem of ray tracing really reduces to the problem of determining the best method of carrying out a numerical approximation.

2. MODELING THE OCEAN ENVIRONMENT

2.1 Treatment of the Sound-Speed Field

Presently GRASS has four programs (DTSTOV, VFC, PRFPLT, and CTOUR) for interpolating, extrapolating, and displaying the sound-speed field (Fig. 1). Although each program is complete in itself, its major input, with the exception of DTSTOV, is the output of another program. Currently the media of intercommunication is cards and magnetic tape.

2.1.1 Conversion of Depth, Temperature, and Salinity Data to Sound-Speed Profiles (DTSTOV Program)

2.1.1.1 Purpose

Frequently the prospective user of GRASS has only salinity, temperature, and depth (STD) data at his disposal, obtained by XBT's, AXBT's, and/or Nansen casts. At any rate it is necessary to convert these to sound-speed profiles. DTSTOV uses Leroy's second equation, Eq. (7) of Ref. 35, to provide this conversion capability:

$$c = \sum_{i=1}^{5} \tilde{c}_i , \tag{4}$$

where

$$\tilde{c}_1 = 1493 + 3(T - 10) - 6 \times 10^{-3}(T - 10)^2 - 4 \times 10^{-2}(T - 18)^2 + 1.2(S - 35) - 10^{-2}(T - 18)(S - 35) + \frac{z}{61} ,$$

$$\tilde{c}_2 = 10^{-1}\zeta^2 + 2 \times 10^{-4}\zeta^2(T - 18)^2 + 10^{-1}\zeta \frac{L}{90} ,$$

$$\tilde{c}_3 = 2.6 \times 10^{-4} T(T - 5)(T - 25),$$

$$\tilde{c}_4 = - 10^{-3}\zeta^2(\zeta - 4)(\zeta - 8),$$

$$\tilde{c}_5 = 1.5 \times 10^{-3}(S - 35)^2(1 - \zeta) + 3 \times 10^{-6} T^2(T - 30)(S - 35)$$

and

c is the sound speed (m/s),

T is the temperature (°C),

S is the salinity (%),

z is the depth (m)

ζ is the depth (km),

L is the latitude (degrees).

For salinities greater than 30‰ the $\tilde{c}_5$ term of Eq. (4) is omitted.

The user of DTSTOV has the option of printing out the pressure (kg/cm^2) corresponding to each depth. Leroy's geographically dependent pressure equations derived empirically from many different areas [36] are used for this calculation.

2.1.1.2 Input

A free-field input routine [37] reads in IBM cards containing the STD data and their corresponding lattitude and longitudes and containing output-control and data-identifying parameters. If the data do not fall within the following limits, the program prints out an error message and stops: salinity, 20 to 42‰; temperature, −2 to 34°C; and depth, 0 to 10,000 meters. There is no limit to the number of STD profiles that may be read in.

2.1.1.3 Output

The printer listing shows the profile ranges, latitudes, longitudes, depths, temperatures, salinities, and sound speeds. Pressures may be printed as a user option. In addition the minimum and maximum depths, temperatures, and salinities are printed for each profile.

Each profile's range (n.mi.), latitude and longitude (deg and min), temperature (°C), and salinity at its maximum depth of observation (MDO) and its depth-and-sound-speed pairs are punched on cards. The MDO temperature and salinity are punched to facilitate later extension of the profile to the ocean bottom by the VFC program.

2.1.1.4 Accuracy

Wilson's [38] second equation is widely used to calculate the speed of sound in seawater. Leroy [35] proposed two formulas: one that approximates Wilson's equation and one that approximates the data Wilson used when computing his second formula. These formulas are simple and fairly accurate; in fact Leroy has demonstrated that Eq. (4), his second equation, fits Wilson's data better than Wilson's equation itself. Another advantage of Leroy's equation is that it gives sound speed as a function of depth, temperature, and salinity and thus avoids the intermediate and time-consuming conversion of depth to pressure required by Wilson's equation.

Equation (4) has been divided into five parts [39]:

- A minimum number of terms $\tilde{c}_1$ forming the "simplified" formula, which is sufficient with a slightly reduced accuracy for depths of less than 1000 m at any latitude provided that $T < 25°C$ and $30‰ < S < 42‰$.

- A depth-, temperature-, and latitude-dependent expression $\tilde{c}_2$ which is necessary for depths greater than 1000 m. It extends the validity of the formula to depths of 7000 m and improves the accuracy to ±0.1 m/s (for $T \leqslant 23°C$).

- A temperature correction $\tilde{c}_3$ for $T \geqslant 25°C$. This correction still leaves the results at lower temperatures within 0.1 m/s of Wilson's formula and permits the calculation of sound speeds for temperatures up to 34°C.

- A correction term $\tilde{c}_4$ for very great depths, necessary only for depths greater than 7000 m.

- A corrective term $\tilde{c}_5$ for low salinity to be applied only when $S < 30‰$.

In calculating Eq. (4) DTSTOV uses double-precision arithmetic to avoid roundoff errors.

2.1.1.5 Recommendations for Improvement

Frye and Pugh [40] derived an 11-term empirical sound-speed equation which is a significant improvement over the published equations of Wilson. Unfortunately this equation is valid only for salinities less than 36.6‰. Although the authors claim this equation is valid over 99.5 percent of the open-ocean volume, it does not apply in important areas like the Mediterranean Sea, where the salinities lie in the vicinity of 38‰. Currently Frye and Pugh are acquiring new data to extend the domain of their equation, but until that equation is published we have decided to use Leroy's.

Concerning experimental data collection, the need exists for real-time computer collection of depth, temperature, salinity, and sound-speed data. For example, at this time it is relatively straightforward to interface an XBT recorder through an analog-to-digital recorder to a minicomputer. As the XBT is being dropped, the computer could be digitizing the temperature profile according to adaptive algorithms, similar to those suggested by Rattray [41], for determining optimum sampling depths and storing the results on magnetic tape. These algorithms tell the user how he should interpolate between the data points, in addition to giving him a minimum number of points. The standard practice today is to give the user an array of numbers and let him figure out how to interpolate between them.

2.1.2 Interpolation and Extrapolation of the Sound-Speed Field (VFC Program)

2.1.2.1 Purpose

The purpose of the VFC (velocity-field construction) program is:

- To examine the input bottom-topography and sound-speed data for consistency and physical meaningfulness. Unusually large gradients and curvatures are flagged. Other inconsistencies may result in warning messages and possible termination of execution.

- To extend all input sound-speed profiles to the ocean bottom.

- To correct, if requested, the extended sound-speed profiles and bottom depths for earth curvature.

- To determine the first and second derivatives of the interpolated and extrapolated sound-speed-field data.

- To generate a magnetic tape (coefficient tape) containing the bottom profile and the sound-speed field and its derivatives for input to other programs in the system.

2.1.2.2 Input

All input data to the VFC program are punched on cards in free-field format. They include:

- Program-control parameters and data identification numbers.

- The bottom topography in the form of up to 1000 nonuniformly spaced range-and-depth pairs in user-defined units. The program assumes a linearly segmented bottom.

- The sound-speed profiles. Each profile may have up to 1000 nonuniformly spaced depth-and-sound-speed pairs. There are no limitations on the number of profiles, the ranges of the profiles, the maximum depths of observations, or the units of measurement.

2.1.2.3 Output

The output consists of:

- A magnetic tape (coefficient tape) containing the corrected and extended sound-speed profiles and their corresponding first and second derivatives and the bottom topography.

- A printer listing containing control parameters, data identification numbers, and error and warning messages. Optional output includes: listings and printer plots of the input sound-speed profiles, a listing and printer plot of the bottom profile corrected for earth's curvature, listings and printer plots of the final corrected and extended profiles, and listings of the first and second derivatives, that is, the vertical gradients and curvatures.

2.1.2.4 Interpolation in Depth

The VFC program uses a combination of cubic-spline and linear interpolation schemes to model the sound-speed field. This representation differs significantly from that used in the HLRTP and most other ray-tracing programs.

Interpolation in depth is carried out using cubic splines [42-43]. The mathematical model of the cubic spline is as follows: Let $z_1, z_2, \ldots, z_n$ be distinct, not necessarily uniformly spaced, depths such that

$$a = z_1 < z_2 < z_3 \ldots < z_n = b$$

and let $c_1, c_2, \ldots, c_n$ be the sound speeds corresponding to these depths. In our application the depth a is normally, zero. The cubic-spline function $f(z)$, for $a \leq z \leq b$, has the following properties:

1) $f(z_i) = c_i$, $i = 1, 2, \ldots, n$. The spline passes through all the input data points.

2) $f(z)$, $f'(z)$, and $f''(z)$ are continuous.

3) In each interval $[z_i, z_{i+1}]$, $i = 1, \ldots, n-1$, $f(z)$ is a cubic polynomial.

4) If $g(z)$ is any other function satisfying properties 1 through 3, then*

$$\int_a^b [f''(z)]^2\, dz \leq \int_a^b [g''(z)]^2\, dz\,. \tag{5}$$

One can show that property 4 is satisfied provided

$$f''(a) = f''(b) = 0.$$

Since $f(z)$ is cubic, $f''(z)$ is linear in the interval $z_i \leq z \leq z_{i+1}$. That is,

$$f''(z) = f''(z_i) + (z - z_i)\,\frac{[f''(z_{i+1}) - f''(z_i)]}{z_{i+1} - z_i}\,. \tag{6}$$

Hence, if we can determine $f''(z)$ for $i = 2, \ldots, n-1$, we can determine $f(z)$, $f'(z)$, and $f''(z)$ anywhere on the interval $[a, b]$ by straightforward integration of Eq. (6).

By introducing the notation

$$h_i = z_{i+1} - z_i,\ i = 1, 2, \ldots, n-1,$$

$$f_i'' = f''(z_i),\ i = 1, 2, \ldots, n,$$

$$c[i+1, i] = \frac{c_{i+1} - c_i}{h_i}\,,\ i = 1, 2, \ldots, n-1,$$

we can show [42, 43] that solving for the curvature f_i'' reduces to the problem of solving the system of linear equations

$$HF = D, \tag{7}$$

*If one considers the spline $f(z)$ to represent a flexible strip of plastic or wood (a mechanical spline), the potential energy of that strip would be proportional to the integral of the square of the curvature $f''(z)$. Hence minimizing the potential energy is equivalent to minimizing $\int_a^b [f''(z)]^2 dz$.

where

$$H = \begin{pmatrix} 2(h_1 + h_2) & h_2 & 0 & \cdots & 0 \\ h_2 & 2(h_2 + h_3) & h_3 & 0 & \cdots \\ 0 & h_3 & 2(h_3 + h_4) & \cdots & 0 \\ \cdots & 0 & \cdots & \cdots & h_{n-2} \\ 0 & \cdots & 0 & h_{n-2} & 2(h_{n-2} + h_{n-1}) \end{pmatrix}$$

$$F = \begin{pmatrix} f''_2 \\ f''_3 \\ \cdots \\ f''_{n-1} \end{pmatrix},$$

$$D = 6 \begin{pmatrix} c[3, 2] - c[2, 1] \\ c[4, 3] - c[3, 2] \\ \cdots \\ c[n, n-1] - c[n-1, n-2] \end{pmatrix}$$

Note that H is a symmetric, tridiagonal, positive-definite, diagonally dominant, $(n - 2)$-by-$(n - 2)$ matrix. To solve this linear system, we use the method of successive overrelaxation suggested by Greville [42].

The cubic spline has several advantages over other methods of interpolation:

- In the sense of satisfying Eq. (5) the cubic spline is the smoothest function which interpolates the given data.

- It yields continuous first and second derivatives.

- Its characteristics and error bounds are well understood. (Further discussion of splines, including error analysis, may be found in Refs. 44 and 45).

One disadvantage of the cubic spline, correctly pointed out by Weinberg [31b], is that it can yield erroneous values of sound speed if precautions are not taken. To help avoid these erroneous values, the VFC program flags unusually large gradients and curvatures. "Unusually large" is defined by the user in the form of input parameters. Typically an unusually large gradient would be one whose magnitude exceeded 1 s^{-1} and an unusually large curvature would be one which exceeded 0.1 m^{-1} s^{-1}. To be safe, the user may plot

his profiles using PRFPLT and see exactly how the program will interpolate between data points. If erroneous values of sound speed are detected, the user can delete or add points and thereby force the spline to give a physically more meaningful representation. In the future an algorithm could be implemented that automatically carries out these deletions and additions, based on the input parameters mentioned. That is, the interpolation procedure could be modified to take into account the maximum and minimum gradients and curvatures likely to appear in a given region. These maxima and minima will of course be depth dependent. As an alternative approach one could replace the pure cubic spline with the least-squares cubic spline proposed by Powell [46]. Because Powell's technique does not insist on property 1 of Section 2.1.2.4, the resulting least-squares spline can have more physically meaningful curvatures than the cubic spline. The use of such a technique would probably diminish the difficulties pointed out by Weinberg. Additional recommendations will be given in Section 2.1.2.9.

Weinberg [31b] claims that his continuous-gradient technique is superior to the pure cubic spline for a sound-speed field having only a depth dependence. This may indeed be true, but the following points bear mentioning:

- The Weinberg technique does not have second-derivative continuity and thus is somewhat less desirable from a theoretical point of view. Although it may be true, as Weinberg suggests, that in most practical applications this is of no consequence, nevertheless Pedersen [32] has shown that discontinuities in the second derivative lead to the infinite rates of change of intensity mentioned in Section 1.3.

- Curve fitting using a cubic spline is more straightforward than the Weinberg technique.

The method used in the HLRTP for representing the sound-speed field was initially implemented and later discarded because it led to unrealistic variations of the profile curvature and is physically and mathematically less appealing than the cubic spline. Moler and Solomon [47] discuss the use of cubic splines in a ray-tracing program having only a depth-dependent sound-speed field.

2.1.2.5 Interpolation in Range

Consider the interpolation of the sound-speed field and its derivatives at a point between two input profile ranges. In particular consider a point at range R, $R_1 < R < R_2$, and depth z, where R_1 and R_2 are two adjacent input profile ranges.

Let $f(R, z)$ be a two-dimensional interpolation function corresponding to the one-dimensional function $f(z)$ of the previous section. We use linear interpolation to approximate a value of sound speed at the point (R, z) as follows:

$$f(R, z) = f(R_1, z) + (R - R_1)\frac{[f(R_2, z) - f(R_1, z)]}{R_2 - R_1} \tag{8}$$

where the values of f at the arguments (R_1, z) and (R_2, z) are obtained by the cubic-spline technique. Similarly, replacing each occurrence of f in Eq. (8) with f_z, and f_{zz}, we can obtain approximations for the vertical gradient and curvature respectively at the point (R, z).

To estimate the horizontal gradient f_R at the point (R, z) we use the first finite divided difference:

$$f_R(R, z) = \frac{[f(R_2, z) - f(R_1, z)]}{R_2 - R_1}. \tag{9}$$

Thus we can obtain approximations for f, f_z, f_{zz}, and f_R at any point (R, z) in the range-and-depth plane.

2.1.2.6 Earth-Curvature Correction

If we consider the earth to be a sphere of radius a and pass a plane through the center of this sphere, we can describe the position of any point p at range r and depth q by the complex number z, where $z = x + iy$. In the polar coordinates of Fig. 5 we have, since $r = a\theta$,

$$z = (a - q)e^{ir/a}. \tag{10}$$

The set of equations

$$u = u(r, q),$$

$$v = v(r, q)$$

defines a transformation which establishes a correspondence between points in the z and w planes. (In these next few paragraphs we will reiterate some of the discussion given in Ref. 48.) If u and v are continuously differentiable and the Jacobian $\partial(u, v)/\partial(x, y)$ does not vanish in a region R, then the transformation is one to one in R. A special case occurs when u and v are the real and imaginary parts of an analytic function of a complex variable $z = x + iy$, namely, $w = u + iv = f(z) = f(x + iy)$. In this case the Jacobian of the transformation is given by

$$\frac{\partial(u, v)}{\partial(x, y)} = |f'(z)|^2.$$

Hence it follows that the transformation is one to one in regions where $f'(z) \neq 0$.

Consider the definition of a conformal mapping. If under a transformation a point (x_0, y_0) of the z plane is mapped into a point (u_0, v_0) of the w plane, while curves C_1 and C_2 intersecting at (x_0, y_0) are respectively mapped into curves C_1' and C_2' intersecting at (u_0, v_0); then if the transformation is such that the angle at (x_0, y_0) between C_1 and C_2 is equal to the angle at (u_0, v_0) between C_1' and C_2' both in magnitude and sense, the transformation is said to be conformal at (x_0, y_0). A fundamental theorem of complex-variable theory states that if $f(z)$ is analytic and $f'(z) \neq 0$ in a region R, then the mapping $w = f(z)$ is conformal at all points of R.

We now consider a transformation, namely,

$$w = ae^{-i\pi/2} \ln (z/a) = u + iv. \tag{11}$$

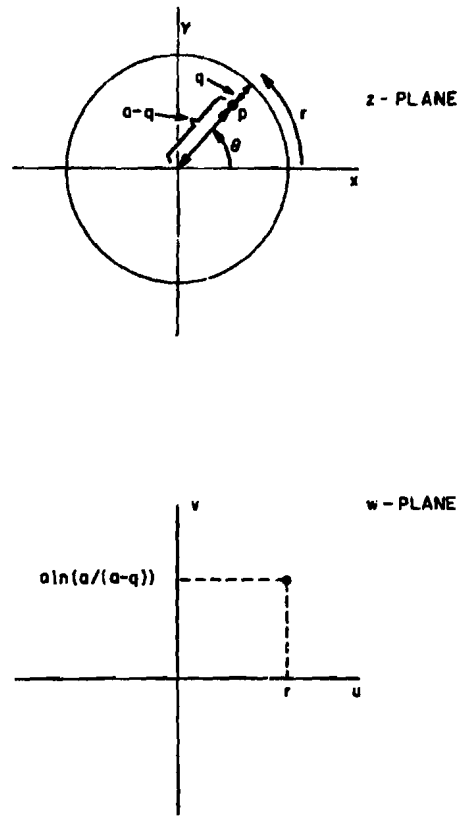

Fig. 5—Planes for the earth-curvature correction

This function is analytic at all finite values of z except at $z = 0$, where the derivative does not exist. The point $z = 0$ is called a singular point of w. Clearly w is conformal at all points of the region R provided R is defined as excluding the point $z = 0$. This point is of no interest in our calculations.

Combining Eqs. (10) and (11),

$$w = r - ia \ln [(a - q)/a] = u + iv. \tag{12}$$

An interesting feature of this transformation is that it maps the circumferential coordinate r into the linear coordinate u and maps the depth coordinate q into the v coordinate, which is independent of r. To see why this occurs, note that Eq. (11) first compresses the region R by the factor a and then uses the log function to map the resulting annular region into a rectangular region. This rectangular region is then rotated clockwise 90 degrees and stretched by the factor a.

Expressing the speed of sound at the point p in polar coordinates of the z plane, we have

$$c_z = \sqrt{(a-q)^2\left(\frac{d\theta}{dt}\right)^2 + \left[\frac{d(a-q)}{dt}\right]^2}$$
$$= \sqrt{\left(\frac{a-q}{a}\right)^2\left(\frac{dr}{dt}\right)^2 + \left(\frac{dq}{dt}\right)^2}. \tag{13}$$

In the w plane at a point corresponding to the point p of the z plane, the speed of sound is given by

$$c_w = \sqrt{\left(\frac{du}{dt}\right)^2 + \left(\frac{dv}{dt}\right)^2}$$
$$= \sqrt{\left(\frac{dr}{dt}\right)^2 + \frac{a^2}{(a-q)^2}\left(\frac{dq}{dt}\right)^2}. \tag{14}$$

Hence if one measures a sound speed in the z plane c_z, the corresponding sound speed in the w plane is given by

$$c_w = \frac{a}{(a-q)}\, c_z = e^{v/a}\, c_z, \tag{15}$$

and the coordinates corresponding to range and depth are respectively

$$u = r$$

and

$$v = -a \ln\left(\frac{a-q}{a}\right). \tag{16}$$

These results are identical to those obtained by Watson [49]. Watson however based his derivation on Fermat's principle rather than emphasizing the conformal-mapping aspects of the problem as we have done here. Watson also discussed the implications of earth curvature to three-dimensional ray-tracing problems.

One naturally questions the importance of the earth-curvature correction. As an estimate of the radius a we will take the mean radius of the international spheroid [50], namely, 6.37122935×10^6 meters. Expanding Eq. (16), we have

$$v = -a \ln\left(1 - \frac{q}{a}\right) = a\left(\frac{q}{a} + \frac{1q^2}{2a^2} + \frac{1q^3}{3a^3} + \cdots\right)$$
$$\cong q + \frac{q^2}{2a} = q + \Delta q. \tag{17}$$

In oceanographic work it is highly unusual to consider depths greater than 6000 meters. If, to obtain a worst-case estimate, we let q be 10^4 meters, we see Δq is approximately 7.85 meters. Also c_w is approximately 1.0016 c_z. Since c_z is seldom greater than 1600 m/s, our maximum correction to the sound speed at this depth is about 2.5 m/s. Both of these corrections are likely to be smaller than the experimental uncertainties. Thus for almost all practical purposes the earth-curvature correction can be neglected.

2.1.2.7 Algorithm

The following step-by-step procedure roughly describes how the VFC program works.

1. Initialize certain variables.

2. Read in the bottom topography and write it on the final output tape, and then read in parameters, such as:

TEMPDP—The depth in meters at which for further increases in depth the temperature of the ocean remains approximately constant. This depth serves as the dividing line between "deep" and "shallow" profiles and is normally about 1500 meters. Profiles whose maximum depth of observation (MDO) lies at or below TEMPDP are called "deep."

DPTHMX—The maximum depth allowed in the input data. If an input depth exceeds this depth, the program will print out an error message and stop. All profiles, both deep and shallow, are extended to this depth.

VMIN and VMAX—The minimum and maximum sound speeds permitted in the data. If these are exceeded, the program prints out an error message and stops.

ZMINFL, ZMAXFL, DMINFL, and DMAXFL—The minimum and maximum expected vertical gradients and curvatures. If these are exceeded, the program will print a warning message.

DPINC—The depth interval used in extending the profiles.

3. Read in the next sound-speed profile on cards. The first card for each profile contains its range along the track, its latitude, its longitude, and the temperature and salinity at its MDO. Compare the sound speeds with VMIN and VMAX and check the profile points for proper arrangement.

4. Compare the MDO with TEMPDP to determine if the profile is deep or shallow. If the profile is deep, go to step 5, otherwise go to step 6.

5. If DPINC is not zero, extend the deep profile below the bottom using Leroy's equation, with the temperature and salinity assumed to remain constant at the values described in step 3. Add points to the profile in depth increments of size DPINC meters from the MDO to the depth DPTHMX and check to determine that the resulting profile has no more than 1000 points.

6. If the user requested it, print and printer plot the profile. (These plots are helpful in detecting major errors in the input data; so users are encouraged to examine them carefully before proceeding with ray tracing.)

7. If requested, use Eqs. (15) and (16) to correct the profile for earth curvature.

8. If the profile is shallow, go to step 9. Otherwise calculate the deep profile's second derivatives (curvatures) using the spline technique described in Section 2.1.2.4 and store the depths, sound speeds, and curvatures temporarily on the drum; then go to step 10.

9. Store the shallow profile's depths and sound speeds (not curvatures) in a separate area of the drum. Since the program requires the last profile to be deep, this cannot be the last profile; so go to step 3.

10. If this was the last profile, go to step 11. Otherwise go back to step 3.

11. Write some data-identifying information on the final output tape. Set the flag parameter NPOS to 0.

12. Read the next shallow profile from its temporary storage area on the drum. If there are no more shallow profiles, go to step 26.

13. If the range of the next deep profile on the drum is less than the last-read shallow profile, call it the "before" profile with range R_B and read its depths, sound speeds, and curvatures from the drum. Otherwise the range of the profile is greater than that of the shallow profile, so go to step 15.

14. If requested, print and printer plot this deep profile. Also write its depths, sound speeds, and curvatures on the final output tape. Then go to step 13.

15. Let R_A be the range of the first deep profile after and nearest the shallow profile and let R_S be the range of the shallow profile. In other words, in step 13 and this step find the two deep profiles which are closest to and have ranges R_B and R_A bracketing the shallow profile (Fig. 6). If the flag NPOS is set to 9, restore it to 0 and go to step 16. Otherwise, read in the depths, sound speeds, and curvatures for the after profile from the drum.

16. Use cubic-spline interpolation (the curvatures have already been determined) to obtain a value of sound speed c_{MB} on the before profile at the depth z_{ms} corresponding to the MDO of the shallow profile. Similarly, interpolate a value of sound speed c_{MA} on the after profile at the same depth (Fig. 6).

17. Determine whether the after profile or the before profile has the next lowest depth z in its data. If the after profile has the next lowest depth, then let c_A be its sound speed at this depth and interpolate a value of sound speed c_B on the before profile at the same depth using the cubic spline. If on the other hand the before profile has the next lowest depth z, interpolate a sound speed c_A on the after profile using the cubic spline.

18. To obtain the sound speed $c(R_S, z)$ at depth z on the shallow profile at range R_S, combine the two sound speeds c_A and c_B at depth z as follows. Letting $z^* = 1.1\ z_{MS}$ (the constant 1.1 will be explained later), if z is greater than z^*, then

$$c(R_S, z) = c_B + D_B D_c / D_R, \tag{18}$$

but if z is less than or equal to z^*, then

$$c(R_S, z) = c_B + D_B D_c / D_R - D_I (D_B D_c / D_R + c_{MB} - c_{MS}) / D_z, \tag{19}$$

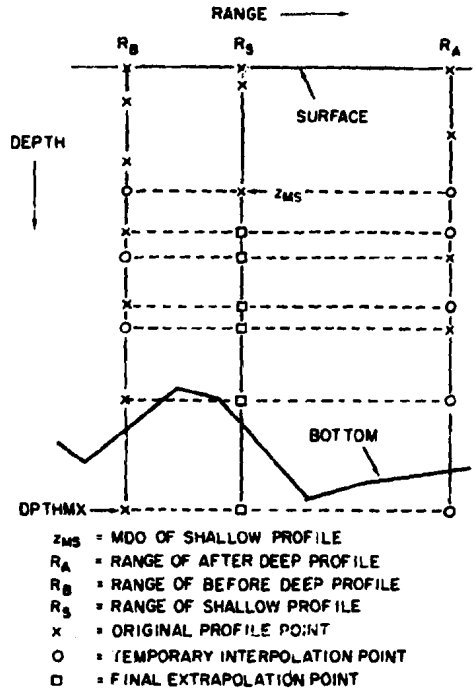

Fig. 6—Extrapolation points of a shallow profile

where

c_{MS} = sound speed of the shallow profile at z_{MS},

c_{MA} = sound speed of the after profile at z_{MS},

c_{MB} = sound speed of the before profile at z_{MS},

$D_B = R_S - R_B$,

$D_R = R_A - R_B$,

$D_c = c_{MA} - c_{MB}$,

$D_l = z^* - z$,

$D_z = z - z_{MS}$.

Equation (18) is a linear interpolation between two bracketing deep profiles. In general the linearly interpolated values will be a satisfactory representation of the true sound-speed field at great depths. It is unlikely however that the interpolated value of the sound speed at the MDO of the shallow profile using Eq. (18) will match the observed value of sound speed at the profile's MDO. For this reason an adjustment [12e] is made by Eq. (19) between the sound speed at the MDO and the sound speeds at greater depths to insure that the extended profile will be continuous. The depth z^* was chosen as the result of experience to be 1.1 times the MDO of the shallow profile. It is assumed that at this depth linear interpolation between the deep profiles is permissible.

19. If the shallow profile has been fully extended to the depth DPTHMX, go to step 20; otherwise go to step 17.

20. Determine the curvatures for the fully extended shallow profile using the cubic-spline technique.

21. Write the extended shallow profile's depths, sound speeds, and curvatures on the output tape. If requested, printer plot the shallow profile and print its first and second derivatives.

22. Read the next shallow profile from the temporary storage area. If there are none go to step 25; otherwise go to step 23.

23. If this new shallow profile is at a range less than the after profile corresponding to the last shallow profile, set the flag NPOS to 9 and go to step 15. Otherwise go to step 24.

24. Write the previous after profile on the final output tape and, if requested, print and printer plot it. Call this "after" profile the "before" profile and go to step 13.

25. Write the last deep profile on the output tape. If requested, printer plot and print the profile.

26. Read the next deep profile and its curvatures from its temporary storage area on the drum. If there are none, go to step 27. Otherwise write the profile on the output tape. If requested, printer plot and print the profile. Repeat this step.

27. End.

2.1.2.8 Sinusoidal-Profile Test Case

Consider the sinusoidal sound-speed profile

$$c = c_0 + A \sin \omega z \tag{20}$$

over the depth interval $0 \leqslant z \leqslant z_m$. For this test case we let $c_0 = 1500$ m/s, $A = 100$ m/s, $\omega = 2\pi/512$ m^{-1}, and $z_m = 1024$ m. The first (gradient) and second (curvature) derivatives of this profile are respectively

$$Z = A\omega \cos \omega z \tag{21}$$

and

$$D = -A\omega^2 \sin \omega z. \tag{22}$$

The profile was sampled eight times per cycle, and the digitized values of Eq. (20) were fed into the VFC program to obtain the first and second derivatives. Table 1 compares the exact gradients and curvatures calculated from Eqs. (21) and (22) with the VFC output. Figure 7 shows the input data points as crosses and the interpolated values of sound speed and its derivatives as solid lines.

Table 1
Results of the Sinusoidal-Profile Test Case

Depth (m)	Sound Speed (m/s)	Exact Gradient (s^{-1})	VFC Gradient (s^{-1})	Exact Curvature (s^{-1} m^{-1})	VFC Curvature (s^{-1} m^{-1})
0	1500.0000	1.22718463	1.22439344	0.000000000	0.00000000
64	1570.7107	0.86775058	0.86577718	-0.010648902	-0.01206758
128	1600.0000	0.00000000	0.00000041	-0.015059821	-0.01584885
192	1570.7107	-0.86775058	-0.86577217	-0.010648902	-0.01206938
256	1500.0000	-1.22718463	-1.22439142	0.000000000	-0.00000001
320	1429.2893	-0.86775058	-0.86577772	0.010648902	0.01206787
384	1400.0000	0.00000000	-0.00000040	0.015059821	0.01584884
448	1429.2893	-0.86775058	0.86577213	0.010648902	0.01206940
512	1500.0000	1.22718463	1.22439144	0.000000000	0.00000001
576	1570.7107	0.86775058	0.86577656	-0.010648902	-0.01206787
640	1600.0000	0.00000000	0.00000000	-0.015059821	-0.01584873
704	1570.7107	-0.86775058	-0.86577656	-0.010648902	-0.01206787
768	1500.0000	-1.22718463	-1.22439375	0.000000000	0.00000000
832	1429.2893	-0.86775058	-0.86577656	0.010648902	0.01206787
896	1400.0000	0.00000000	0.00000000	0.015059821	0.01584873
960	1429.2893	0.86775058	-0.86577656	0.010648902	0.01206787
1024	1500.0000	1.22718463	1.22439375	0.000000000	0.00000000

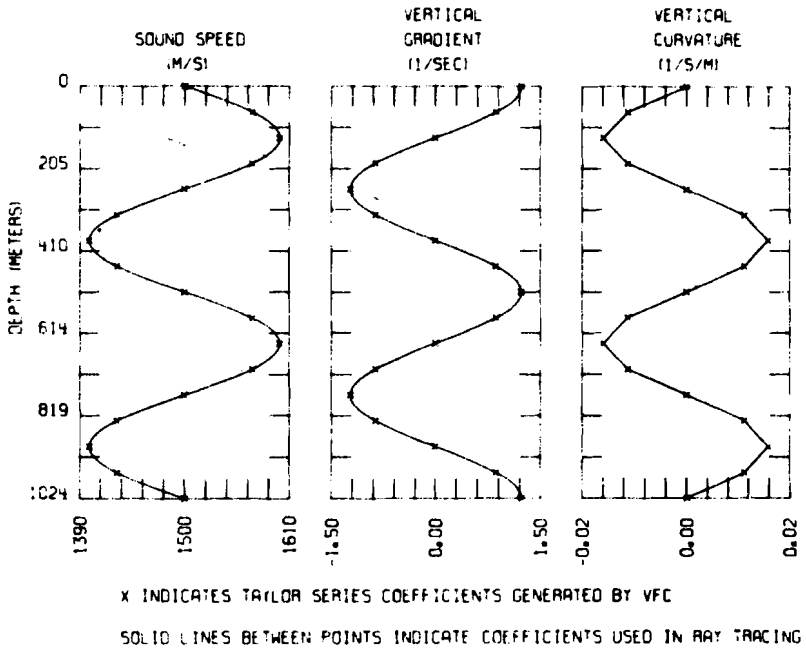

Fig. 7—PRFPLT output for the sinusoidal-profile test case using cubic spline interpolation. The crosses indicate Taylor series coefficients generated by the VFC program, and the solid lines indicate coefficients used in ray tracing.

2.1.2.9 Recommendations for Improvement

The VFC program could be improved in the following ways:

- The efficiency of SERPENT could be increased if a routine were built into the VFC program to determine the minimum number of profile points required to represent the sound speed within experimental accuracy. This increased efficiency would result from reduced search and input/output times.

- The efficiency of SERPENT could be still further increased if all of the profile points were at the same depths, such as standard depths. This efficiency increase would also result from reduced search and input/output times. The coefficient tape would need to have only one array of profile-point depths, rather than an array for each profile. Unfortunately, this same recommendation would limit the ability of the program to accurately represent an arbitrary sound-speed field. This recommendation could possibly be incorporated as an option.

- The program could use two- or even three-dimensional splines [51-53]; rather than the one-dimensional spline discussed. At least one investigator [5] believes that linearly interpolating between sound-speed profiles may not be physically meaningful, because the sound channels do not develop in the manner suggested by linear interpolation. This does not present a serious problem for GRASS, because the system has the ability to handle an unlimited number of sound-speed profiles. By making the spacing between the profiles arbitrarily small, it is possible to achieve any desired degree of accuracy. Admittedly, this procedure will increase program running time and, at times, additional profiles may not be available. Thus the multidimensional spline or some other representation may be preferable. (Of course, determining the coefficients of a multidimensional spline will require more running time and more core storage than those of a one-dimensional spline. Hence multidimensional splines are not without their disadvantages.)

- Along these same lines it would be helpful to know experimentally and by geographical area the depths at which the temperature of the ocean remains nearly constant for further increases in depth. Also a knowledge of the range- and depth-dependent maximum and minimum gradients and curvatures of the sound speed, possibly by season and by geographical area, together with the uncertainties in experimental measurements would be of great value in revising and devising new interpolation schemes.

- The same comments given in Section 2.1.1.5 concerning the need for real-time computer collection of data again apply here.

- The speeds of the VFC, PRFPLT, CTOUR, and SERPENT programs could be increased if the sound-speed profiles and their curvatures and the bottom profile were stored on the disk or the drum rather than on magnetic tape because of the smaller access times and the random access capability of these devices. Unfortunately users of the CDC 3800 are not permitted to store information permanently on the drum. It is possible to use the disk at NRL for permanent storage, however, and the drum can be used for the storage of intermediate results of different runs in the same job. This means that the VFC and SERPENT programs could be combined into one job with the profiles being temporarily stored on the drum. Unfortunately, if SERPENT did not run successfully, possibly because of an input error, the VFC program would have to be run again. On the other hand there would be no difficulty in storing intermediate results permanently on the disk.

2.1.3 Profile Plotting (PRFPLT Program)

2.1.3.1 Purpose

The PRFPLT program generates Calcomp or Gerber [54] plots of sound-speed profiles selected by the user from the coefficient tape. The vertical gradients and curvatures corresponding to a profile are plotted on the same graph as its sound speeds. Examination of these plots will give the user considerable insight into the validity of his data. For example experience has shown that profiles having vertical gradients exceeding 1 s^{-1} or vertical curvatures whose absolute values exceed 0.1 $m^{-1}s^{-1}$ at depths greater than a few hundred meters are probably in error.

2.1.3.2 Input

The input data to the PRFPLT program are on both magnetic tape and punched cards. The magnetic tape is the coefficient tape generated by the VFC program. The punched cards contain:

- The maximum depth of the graph in meters.
- The maximum and minimum values of sound speeds, gradients, and curvatures to be displayed. These values may be determined from the VFC printout.
- Numbers identifying the profiles to be plotted.
- Titles for each of the plots.

2.1.3.3 Output

Figures 7, 8, and 9 are examples of PRFPLT output. The crosses are the values of the profile sound speeds and derivatives which have been entered on the coefficient tape. The solid lines between the crosses are drawn by linearly interpolating between 501 equally spaced points which have been calculated using cubic-spline interpolation. These lines indicate the gradients and curvatures used by SERPENT for ray tracing.

Graphical output may be of one of two forms: Calcomp plots or Gerber plots. The Calcomp plots have the advantage that they are obtained directly and quickly from the computation center. They do not require the services of a special plotter operator or the transportation of tapes to a special plotting facility. Their major disadvantage is that their thin wiggly lines do not reproduce well in reports. The Gerber plotter, on the other hand, has three major advantages. First, it can produce much larger (up to 5 by 8 feet) and more accurate plots than the Calcomp. Second, the plotting is done with India ink pens of the Leroy type on high-quality drawing paper, making a solid black line that reproduces well, even with ozalid or other direct processes. Several pen widths can be used in one program, and different colors of ink can be used. Third, the plotter incorporates a linear interpolator, so that the pen travels in a straight line between successive pairs of plotted xy values, rather than wiggles. The resulting plot is much smoother.

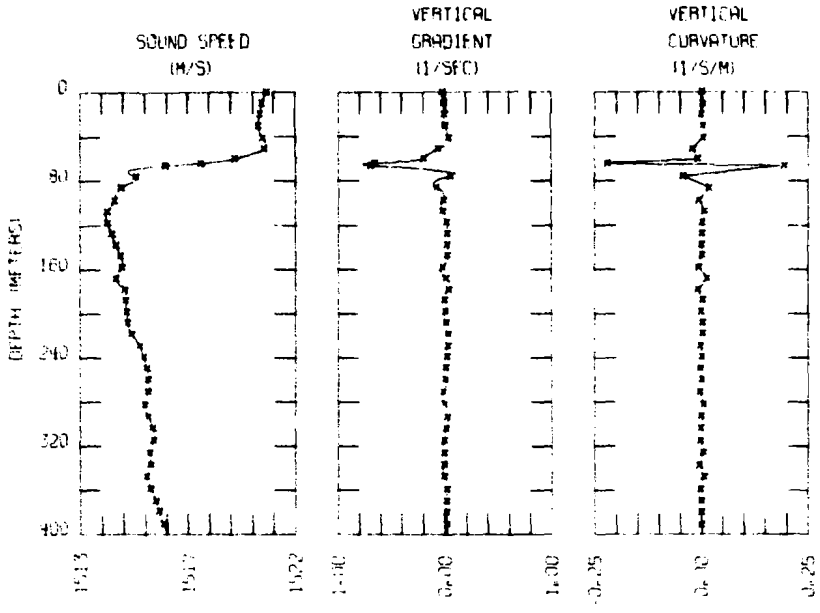

Fig. 8—PRFPLT output for a sound-speed profile derived from XBT measurements in the Ionian basin

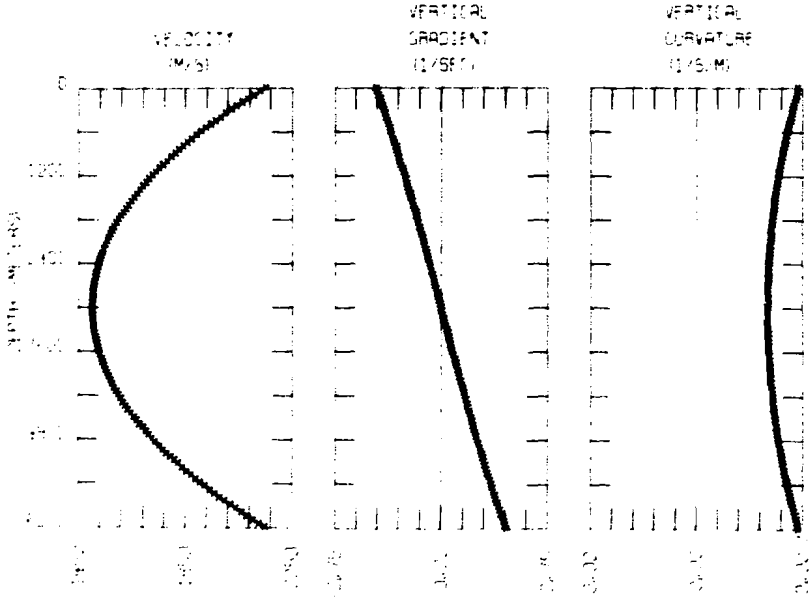

Fig. 9—PRFPLT output for the untilted-hyperbolic-cosine-profile test case using cubic spline interpolation

2.1.4 Contouring and Generating Three-Dimensional Isometric Plots of the Sound-Speed Field (CTOUR Program)

2.1.4.1 Purpose

The CTOUR program arose out of a desire to graphically display the dependence of the sound-speed field on both range and depth, especially the range dependence.

This program contours and draws an isometric plot of the sound-speed field. Its input consists of the coefficient tape and a specification of the dimensions of the range-and-depth grid. The intersections of this grid define the points at which values of sound-speed are interpolated. These interpolated values are plugged into contour [55] and isometric [56] plotting routines. Interpolation is required because the plotting routines require values on a uniform grid whereas the coefficient tape usually contains profiles having points at arbitrary ranges and depths. Up to 50 contour levels may be displayed.

The CTOUR program is designed so that the user can contour any rectangular range-and-depth region in his sound-speed field. Hence it permits a detailed examination of the field. The accuracy of the plots is a function of the accuracy of the input data, the interpolation process, and the dimensions of the grid.

2.1.4.2 Input

The input to CTOUR consists of:

- The coefficient tape generated by the VFC program.
- Contour levels, control parameters, and grid specifications in free-field format on cards.

2.1.4.3 Output

The output consists of:

- A Calcomp or Gerber contour plot of the sound-speed field.
- If the user requests, a listing of the interpolated sound speeds at each intersection of the uniform grid.
- A listing of the input control parameters and contour levels.
- A three-dimensional (isometric) Calcomp or Gerber plot of sound speed versus range and depth in the ocean.

2.1.4.4 Algorithm

Initially the control parameters, contour levels, and grid specifications are read and checked against permissible values. Then the ranges and depths are calculated for each

point of the user-defined grid. Next the program considers each range of the grid and interpolates values of sound speed at the grid depths using Eq. (8).

Once the sound speeds are determined, the contouring subroutine CONTOUR is called and a plot is generated. Then CTOUR sets up the parameters required by the isometric plotting routine PLOTISOM and calls it, and the plot is generated.

2.1.4.5 Test Methods and Results

Figure 2 is a contour plot corresponding to an actual sound-speed field in the vicinity of the Gulf Stream. Figure 3 is a three-dimensional plot corresponding to Figure 2.

Figure 10 is a contour plot of the sound speed corresponding to the range-independent hyperbolic-cosine profile shown in Fig. 9. Since there are no horizontal gradients present, the contour plot is merely a series of unequally spaced horizontal lines.

2.1.4.6 Recommendations for Improvement

Close inspection of Fig. 3 indicates that the hidden-line algorithm used in PLOTISOM does not always work as well as one would like. To improve this situation, PLOTISOM could be replaced by Williamson's [57] routine.

2.2 Treatment of the Ocean Bottom

2.2.1 Representing the Bottom Topography

The ocean bottom is assumed to be linearly segmented and is defined by up to 1000 bottom points at nonuniformly spaced ranges and depths.

2.2.2 Describing the Bottom Losses

SERPENT permits the user to specify up to five curves of bottom loss versus grazing angle. The grazing angle is defined to be the angle an incident ray makes with the bottom. The user may define, by range, up to 100 regions over the length of the bottom topography and indicate which of the curves applies in each region. It is the user's responsibility to provide the curves pertinent to his problem. The particular curves chosen by the user will depend on the frequency of the acoustic source and the type bottom under consideration: rock, mud, sand, etc. The user defines his bottom-loss curves by entering values of dB loss for up to 91 nonuniformly spaced grazing angles. These angles must range from 0 to 90 degrees. SERPENT initializes its own bottom-loss tables by linearly interpolating between the above input losses at each integer degree, so that each internal table has 91 points. When a ray strikes the bottom, its angle of incidence is rounded to the nearest degree, and the loss corresponding to that angle is extracted from the pertinent bottom-loss table and is added to a variable which represents the total bottom loss accumulated by that ray. SERPENT calculates the exact point at which the ray intersects the bottom, the bottom slope at that point, and the angle of ray incidence; if requested, it will print and/or store this information on the ray-statistics tape. It also maintains a count of the number of accumulated bottom hits for each ray, and

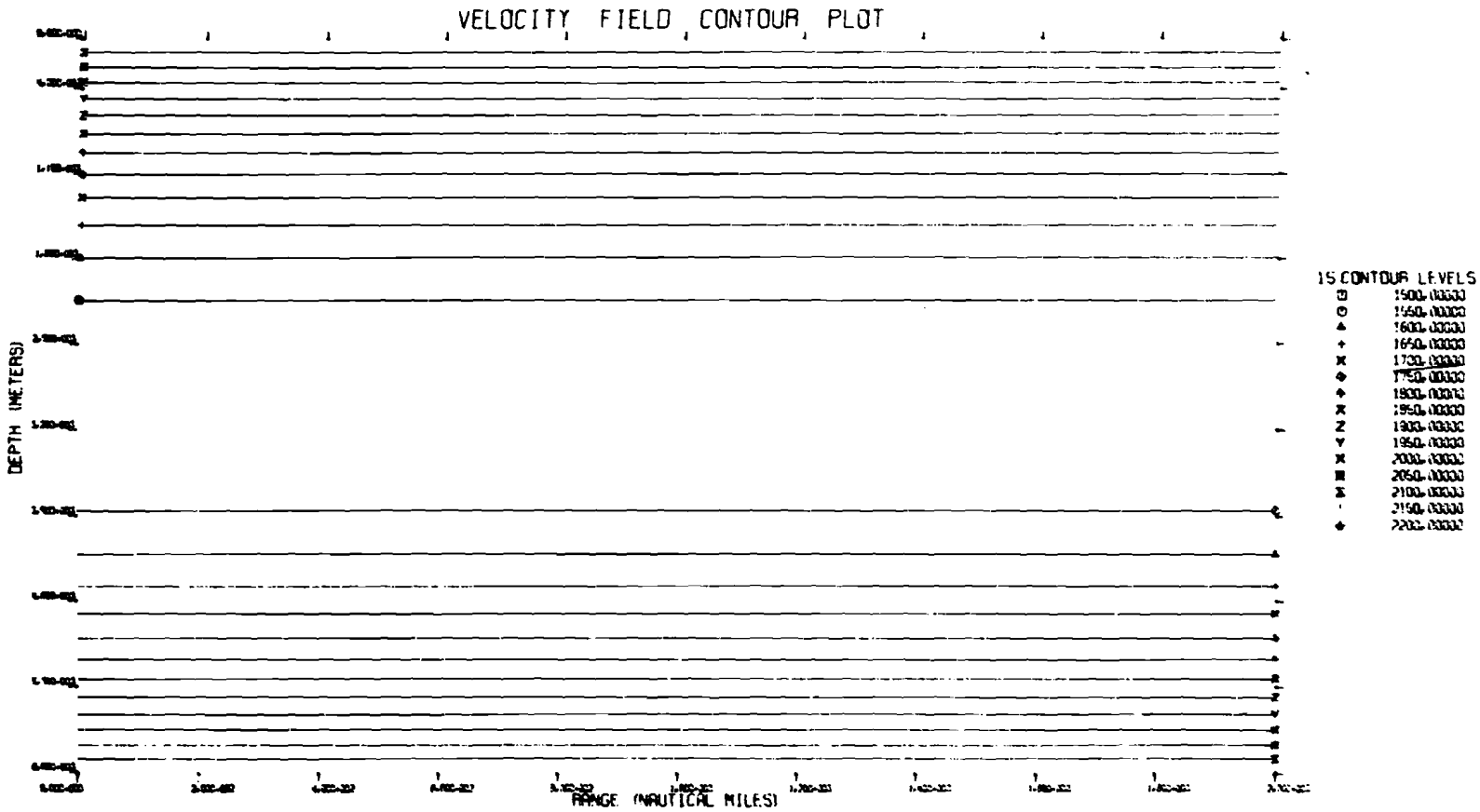

Fig. 10—Contour plot of the untilted-hyperbolic-cosine sound-speed field shown in Fig. 9

terminates a ray if its count exceeds a user-determined limit. Although the program could easily incorporate bottom-reflection phase shifts, it presently has no such provision, since the average user would not likely have these at his disposal in cases of practical interest. The program assumes all rays are specularly reflected. If however a ray is reflected back toward the source, it will be immediately terminated.

2.3 Treatment of the Ocean Surface

2.3.1 Describing the Surface

The surface is assumed to be flat. When a ray strikes the surface, it is specularly reflected and undergoes a phase shift of π radians.

2.3.2 Describing the Surface Losses

A uniform surface loss may be entered in the form of a surface-attenuation parameter. This parameter is the ratio of a ray's intensity after reflection to its intensity before reflection.

If requested, the program will print and/or store on the ray tape the location of each surface hit and the angle of incidence of the ray at that point. The program counts the number of accumulated surface hits for each ray and will terminate a ray when this count exceeds a user-specified limit.

2.4 Treatment of Attenuation

The user may specify the attenuation coefficient α in dB/km (for refracted-only paths) or he may request that the program calculate it for the source frequency using Thorp's equation [58]. Thorp's equation describes the coefficient fairly well for frequencies around and above 1000 Hz. In the calculation of intensity, each arrival is attenuated according to the factor $e^{-\alpha R}$, where R is the range to the receiver. This factor is not exact, because different rays have different total path lengths. We assume that these path differences can be neglected. The ray diagrams tend to exaggerate the path differences, because the depth axis is greatly expanded in comparison to the range axis.

For frequencies about a few hundred hertz or lower, the absorption coefficient is quite small and difficult to measure. Most experiments measure attenuation, rather than absorption, at these frequencies. Attenuation includes everything that is not geometrical spreading. This includes leakage out of the sound channel due to scattering, bottom losses, and nonlinear effects. Hence the users of ray-trace programs must be wary of inadvertently including bottom losses twice in their calculations. That is, they should use attenuation coefficients for only refracted paths.

3. MODELING THE PROPAGATION OF SOUND

3.1 Ray Tracing and Intensity Calculations (SERPENT Program)

3.1.1 Purpose

The SERPENT program has five major functions:

- To trace rays through a two-dimensional range- and depth-dependent sound-speed field bounded by a flat surface and variable bottom topography.

- To provide a comprehensive description of the rays' journey through the inhomogeneous medium.

- To calculate random, coherent, and statistical intensities for multiple receivers at user-selected ranges and depths.

- To generate a transmission-loss tape.

- To generate a ray-statistics tape.

3.1.2 Input

3.1.2.1 Punched Cards

The following input is on punched cards:

- Source information—depth, frequency, beam pattern, intensity of the source along the main beam axis at 1 yard (axial intensity), angular tilt of the main beam lobe, and up to 1500 ray angles.

- Receiver information—up to 1000 ranges and up to 250 depths per range.

- Bottom information—bottom-loss curves, ranges over which loss curves apply, and the maximum number of bottom hits a ray is allowed to experience before being terminated.

- Surface information—attenuation due to a surface hit and the maximum number of surface reflections a ray is allowed to experience before being terminated.

- Output requests—ranges for output, parameters specifying whether to print out complete ray-statistics at each output range, whether to generate a ray tape, whether to calculate intensities, the types of intensity calculations desired, whether to print out the results of intensity calculations, whether to generate a transmission-loss tape, whether to draw printer plots of travel time and/or plots of ray depth versus initial ray angle (ray depth-time distribution plots) at each output range, etc.

- Parameters governing ray iteration—these are discussed in Section 3.1.4.2.

- Run identification information.

All of the above information is read from cards punched in free-field format. For most problems only three or four cards are required.

3.1.2.2 Magnetic Tape

The coefficient tape generated by the VFC program is used for inputting the bottom topography and the sound-speed profiles (Section 2.1.2.3).

3.1.3 Output

The minimum possible output consists of a printer listing of the information punched on the cards described in Section 3.1.2.1 together with a tabulation of the number of profiles, the number of bottom points, the maximum and minimum depth of the bottom topography, and the maximum range of the bottom data contained on the input coefficient tape. The internal bottom-loss tables and the initial ray angles at the source are also listed. Outputs that are optional are described in Sections 3.1.3.1 through 3.1.3.3.

3.1.3.1 Ray-Statistics Magnetic Tape (Optional)

A ray-statistics tape must be generated if one wishes to draw Calcomp or Gerber ray diagrams. This tape is an IBM 729 compatible, seven-track binary tape arranged as follows:

- Logical record 1—80-character title identifying the data.

- Logical record 2—source range, depth, angular frequency, frequency, number of rays, and axial sound level (see Eq. (45) for a definition).

- Logical record 3—initial ray angles.

- Logical record 4—bottom profile ranges, depths, number of bottom points, minimum and maximum depths of the bottom, maximum range of the bottom.

- Logical record 5—iteration-point statistics. (The rays are traced by stepping them from one point in the sound-speed field to the next according to the iteration scheme described in Section 3.1.4. Each of these points is called a ray iteration point. Logical record 5 is repeated for each ray iteration point.) The iteration-point statistics consist of the ray number, ray range, depth, travel time, sine with respect to the horizontal, sound speed at the iteration point, accumulated number of bottom hits, of surface hits, and of turning points, an indicator specifying whether the ray is terminated at this iteration point, and the factors S_i and B_i (see Section 3.1.5.2) containing the accumulated surface- and bottom-loss information for the ray.

To save input/output time and magnetic-tape space, SERPENT combines the data for 222 iteration points and buffers them out in one 2000-word record using a double-buffer technique; that is, while one buffer is filling up, the other is simultaneously being dumped onto magnetic tape.

3.1.3.2 Transmission-Loss Magnetic Tape (Optional)

A transmission-loss tape is required if one wishes to generate Calcomp or Gerber transmission-loss plots. The transmission-loss tape is an IBM 729 compatible, seven-track binary tape and is arranged as follows:

- Logical record 1—number of receiver depths and the values of the receiver depths.
- Logical record 2—ranges at which the above receivers are located.
- Logical record 3—identical to logical record 4 of the ray-statistics tape.
- Logical record 4—identical to logical record 2 of the ray-statistics tape.
- Logical record 5—number of range intervals over which different types of intensity calculations were carried out, maximum range of each interval, types of intensity in each interval, and volume attenuation factor.
- Logical record 6—output range, bottom depth at this range, and types of intensity calculated at this range. This logical record is repeated for each range in logical record 2.
- Logical record 7—transmission losses for each receiver and type of intensity calculation requested for the range in each logical record 6.

3.1.3.3 Printer Listings (Optional)

Since the generation of printer output can significantly increase the program running time, printout options have been built into the program enabling the user to print only those quantities of direct interest, such as intensities.

The user defines the ranges at which he wants information output (printer and/or magnetic tape). He also specifies the parameter NOPRINT. If NOPRINT is set to 0, no ray statistics will be printed. If NOPRINT is set to 1, the following ray statistics will be printed at each of the output ranges:

- Output range in nautical miles and kilometers.
- Bottom depth in meters.
- Ray depths in meters.
- Ray travel times in seconds.
- Accumulated number of surface hits for each ray.
- Accumulated number of bottom hits for each ray.
- Accumulated number of turning points for each ray.
- Termination status of each ray (whether terminated or not).
- Sines of the ray angles at the output range.

- Accumulated ray phase in degrees.
- Location of the surface and bottom hits since the last output range, the bottom slope and grazing angle at each bottom hit, and the angle of incidence at each surface hit.

If the user sets the input parameter NDIST to -1, ray-depth and/or ray-time distribution plots will be generated at each of the output ranges according to whether the parameters NDEPTHDS and NTIMEDS have been set to 0 or 1 respectively. The ray-depth distribution plots are line-printer graphs of ray depth versus initial ray angle at the source for constant range. The ray-time distribution plots are graphs of ray travel time to an output range versus initial ray angle at the source. The slope of a ray-depth distribution plot corresponds to the partial derivative of ray depth with respect to initial ray angle. This derivative appears in the expression for intensity (Eq. (55)). Such a plot shows the depth intervals that are illuminated by individual arrivals, and illustrates which initial angles are mapped into which depths. Ray-depth distribution plots are discussed in more detail in the HLRTP [12f]. The user may specify at which output ranges he would like distribution plots generated.

An option is provided the user for selecting ranges for intensity-calculation printouts. Depending on whether the input parameter NINTENS has been set to 0, 1, or 2, SERPENT will not calculate intensities, will calculate intensities but not print the results, or will calculate intensities and print out the results respectively. If printout is desired, the program will list the intensity, the measured sound level, the transmission loss, and transmission anomaly (Section 3.1.5.2 gives the definitions) at each output range. This printout will also include the number of arrivals at each receiver. The user has the option of defining a set of ranges over which different types of intensity calculations are carried out. For example he can request coherent summation out to 10 nautical miles, random and coherent intensities from 10 to 50 nautical miles, and statistical intensities from 50 to 200 nautical miles. Any combination of random, coherent, and statistical intensity calculations can be carried out in these user-defined regions. The reason for selecting different types of intensity calculations over different range intervals is discussed in Ref. 12g.

3.1.4 Ray-Tracing Theory

3.1.4.1 Derivation of the Iteration Algorithm

The derivation described herein is believed to be unique to this report and is based on an iteration technique discussed by Montagnino [59]. (Basic ray theory is covered in the Appendix.) This derivation differs from that given in the HLRTP [12h] and leads to a similar but more general set of iteration equations. The differences occur in the third- and fourth-order terms of the expansions in ray arc length for the ray range, depth, and travel time. This derivation is not restricted to a particular functional form of the sound-speed field as is characteristic of most derivations. The functional form of the sound-speed field we chose was motivated by considerations of physical meaningfulness and convenience of implementation. There is no reason why one could not use two-dimensional splines to represent the sound-speed field. Indeed there is no theoretical reason why this derivation, or the entire program for that matter, could not be extended to a three-dimensional field. The HLRTP [12i] cites why, in the case of small bottom interaction, there would be no more than a formal advantage in this extension.

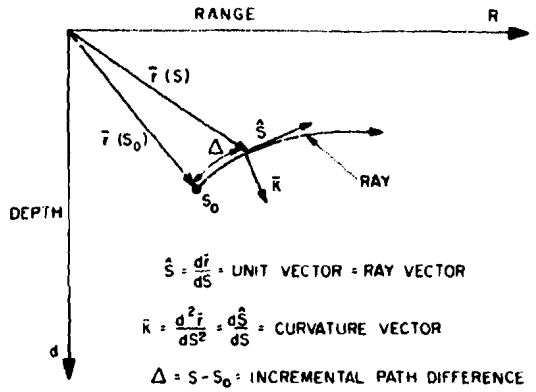

Fig. 11—Iteration of a ray

Consider a curve described by the position vector $\mathbf{r}(S)$, where Δ is the path length measured from some arbitrary point on the ray trajectory S_0 (Fig. 11). According to Taylor's theorem, if we assume $\mathbf{r}(S)$ has $n + 1$ continuous derivatives, the position of a point on the trajectory in the neighborhood of the point $\mathbf{r}(S_0)$ can be written exactly in the form

$$\bar{\mathbf{r}}(S) = \bar{\mathbf{r}}(S_0) + \sum_{i=1}^{n} \frac{\mathbf{r}^{(i)}(S_0)\Delta^i}{i!} + \frac{\bar{\mathbf{r}}^{(n+1)}(\xi)\Delta^{n+1}}{(n+1)!}, \tag{23}$$

where ξ lies somewhere between S and S_0, $\bar{\mathbf{r}}^{(n)}(S_0)$ is the nth derivative of $\bar{\mathbf{r}}$ (S) evaluated at S_0, and $\Delta = S - S_0$ is an increment in the ray-path length from S_0.

Since (Appendix)

$$\bar{\mathbf{r}}^{(1)}(S_0) = \left.\frac{d\bar{\mathbf{r}}}{dS}\right|_{S_0} = \hat{\mathbf{S}}(S_0) = \text{initial ray vector} \tag{24}$$

and

$$\bar{\mathbf{r}}^{(2)}(S_0) = \left.\frac{d\hat{\mathbf{S}}}{dS}\right|_{S_0} = \bar{\mathbf{K}}(S_0) = \text{initial ray curvature,} \tag{25}$$

then

$$\bar{\mathbf{r}}(S) = \bar{\mathbf{r}}(S_0) + \hat{\mathbf{S}}(S_0)\Delta + \frac{\bar{\mathbf{K}}(S_0)}{2!}\Delta^2 + \frac{1}{3!}\left.\frac{d\bar{\mathbf{K}}}{dS}\right|_{S_0}\Delta^3 + \cdots. \tag{26}$$

Equation (26) gives the change in depth and range of a ray in an iteration of size Δ.

Differentiation [59] of Eq. (26) yields the ray vector, or sine and cosine of the ray angle, at the next iteration point, namely,

$$\hat{\mathbf{S}}(S) = \hat{\mathbf{S}}(S_0) + \overline{\mathbf{K}}(S_0)\Delta + \frac{1}{2!}\left.\frac{d\overline{\mathbf{K}}}{dS}\right|_{S_0}\Delta^2 + \cdots . \tag{27}$$

To implement Eqs. (26) and (27), we need expressions for $\hat{\mathbf{S}}(S_0)$, $\overline{\mathbf{K}}(S_0)$, $d\overline{\mathbf{K}}/dS|_{S_0}$, etc.

The ray vector at the initial point S_0 is given by

$$\hat{\mathbf{S}}(S_0) = \gamma\hat{\mathbf{i}} + \sigma\hat{\mathbf{j}}, \tag{28}$$

where

$\gamma = \cos\theta_0$,

$\sigma = \sin\theta_0$,

θ_0 = ray angle at the initial point (positive angles measured downward from the horizontal),

$\hat{\mathbf{i}}$ = a horizontal unit vector,

$\hat{\mathbf{j}}$ = a vertical downward-pointing unit vector.

To obtain $\overline{\mathbf{K}}(S_0)$ and its derivatives, we apply Eq. (A20), namely,

$$\overline{\mathbf{K}}(S) = \frac{1}{\eta}[\nabla\eta - \hat{\mathbf{S}}(\nabla\eta\cdot\hat{\mathbf{S}})], \tag{29}$$

where η is the index of refraction.

We can approximate the sound-speed field $c(S)$ in the vicinity of the point S_0 by a Taylor's series expansion about that point:

$$\begin{aligned} c(S) = c(R,z) \approx\ & c(R_0, z_0) + Z(R_0, z_0)(z - z_0) + D(R_0, z_0)(z - z_0)^2/2 \\ & + G(R_0, z_0)(R - R_0), \end{aligned} \tag{30}$$

where R_0 and z_0 are the range and depth at the point S_0, c is the sound speed, Z is the sound-speed vertical gradient, D is the vertical curvature, and G is the horizontal gradient. These quantities may be obtained from Eqs. (8) and (9) for any point in the sound-speed field as explained in Section 2.1.2.5.

The index of refraction η is given by

$$\eta(S) = \frac{a_0}{c(S)}, \tag{31}$$

where a_0 is a reference sound speed. Our final equations will be independent of the particular value of a_0.

Using Eq. (30) and assuming

$$z - z_0 \approx \sigma\Delta$$

and

$$R - R_0 \approx \gamma\Delta,$$

we have

$$\eta(S) \approx \frac{a_0}{a_1 + a_2\Delta + a_3\Delta^2}, \tag{32}$$

where

$$a_1 = c(R_0, z_0),$$
$$a_2 = z(R_0, z_0)\sigma + G(R_0, z_0)\gamma,$$
$$a_3 = D(R_0, z_0)\sigma^2/2.$$

The gradient of the index of refraction $\overline{\nabla}\eta$ is approximately,

$$\overline{\nabla}\eta(S) \approx b_1\hat{\mathrm{i}} + (b_2 + b_3\Delta)\hat{\mathrm{j}}, \tag{33}$$

where

$$b_1 = \frac{-a_0 G(R_0, z_0)}{a_1{}^2},$$

$$b_2 = \frac{-a_0 Z(R_0, z_0)}{a_1{}^2},$$

$$b_3 = \frac{-a_0 \sigma D(R_0, z_0)}{a_1{}^2}.$$

Assuming the ray vector $\hat{\mathrm{S}}$ at the new point located an arc-length distance Δ from S_0 is given approximately by

$$\hat{\mathrm{S}}(S) \approx \gamma\hat{\mathrm{i}} + \sigma\hat{\mathrm{j}}, \tag{34}$$

we have the ray curvature, Eq. (29),

$$\overline{\mathrm{K}}(S) \approx \sum_{k=1}^{4} \Delta^{k-1}(e_k\hat{\mathrm{i}} + f_k\hat{\mathrm{j}}), \tag{35}$$

so that

$$\overline{\mathrm{K}}(S_0) \approx (d_1\hat{\mathrm{i}} + d_3\hat{\mathrm{j}})a_1 a_0^{-1}, \tag{36}$$

$$\left.\frac{d\overline{\mathrm{K}}}{dS}\right|_{S_0} \approx a_0^{-1}[(a_1 d_2 + a_2 d_1)\hat{\mathrm{i}} + (a_1 d_4 + a_2 d_3)\hat{\mathrm{j}}], \tag{37}$$

$$\left.\frac{d^2\overline{K}}{dS^2}\right|_{S_0} \approx 2a_0^{-1}[(a_2d_2 + a_3d_1)\hat{i} + (a_2d_4 + a_3d_3)\hat{j}] , \tag{38}$$

$$\left.\frac{d^3\overline{K}}{dS^3}\right|_{S_0} \approx 6a_3a_0^{-1}(d_2\hat{i} + d_4\hat{j}) , \tag{39}$$

where

$$d_1 = b_1\sigma^2 - \sigma\gamma b_2,$$
$$d_2 = -\sigma\gamma b_3,$$
$$d_3 = b_2\gamma^2 - \sigma\gamma b_1,$$
$$d_4 = \gamma^2 b_3.$$

To obtain an iteration equation for the travel time, we note

$$T(S) = T(S_0) + \int_{S_0}^{S} \frac{dS}{c(S)} . \tag{40}$$

Expanding $1/c$ in a third-order Taylor series in Δ, we obtain

$$T(S) \approx T(S_0) + \sum_{i=0}^{3} \frac{A_i\Delta^{i+1}}{(i+1)} , \tag{41}$$

where

$$A_0 = a_1^{-1},$$
$$A_1 = -a_2a_1^{-2},$$
$$A_2 = (a_2{}^2 - a_3a_1)a_1^{-3},$$
$$A_3 = a_2(2a_3a_1 - a_2{}^2)a_1^{-4} .$$

The travel-time integral could have been solved exactly instead of making an approximation for $1/c$, but the resulting exact solution would require more computation time than the expansion (41), except in special cases.

The ray plots shown in this report are *not* the result of the equations derived in this section. Rather they resulted from direct implementation of the iteration equations given in the HLRTP [12h]. We have chosen to include the derivation of Eqs. (23) through (41) because it illustrates how equations of the type given in Ref. 12h can be derived. Originally it was an attempt to verify the equations given in Ref. 12h. Unfortunately the authors of the HLRTP did not choose to include a detailed derivation of their iteration equations, and it is not immediately obvious how the third- and fourth-order terms in Δ given in that report were derived.

After further analysis it is expected that the equations given in this section will replace those currently implemented. This topic will be considered again in Section 3.1.7.

3.1.4.2 Accuracy and Iterative Controls

SERPENT requires the user to specify certain "ray tuning parameters" and thereby allows him to make a tradeoff between accuracy and computer running time. These parameters establish the limits for the built-in program controls which adapt the ray arc-length iteration increment Δ to the structure of the sound-speed field. Both the accuracy (up to a point) and running time increase with decreasing parameter sizes.

The user of SERPENT is cautioned against performing a highly accurate calculation on data which because of the natural variability of the oceanographic environment and the uncertainties or meagerness of the measurements may not be representative of the environment at the time of the experiment. Highly accurate calculations are however of value in comparing program results with exact analytic solutions. Comparisons with exact solutions will give the user insight into the operation and interaction of the ray iteration parameters. From another point of view, the program could be used to confirm the correctness of newly developed closed-form analytic solutions.

We will now briefly consider each of the ray iteration parameters. These are identical to the ones discussed in more detail in the HLRTP report [1.2j]. The parameters are:

- Δ_M (DELMAX) and Δ_m (DELMIN)—the maximum and minimum step size (in meters) along the ray arc. If Δ_M is too large, the program will have to reduce Δ a number of times to find a satisfactory step size. If Δ_m is too small, clearly the program will have to perform a large number of calculations to accomplish a given iteration task. Too large a Δ could lead to a breakdown of the iteration expansions. Thus there are optimum values for Δ_M and Δ_m. Currently these are determined by user experience. In practice, using oceanographic data, values for Δ_M up to 1000 m lead to satisfactory operating conditions. Typically Δ_m is set to about the minimum depth interval between input sound-speed profile points, such as 20 m.

- ϵ (VFAEPS)—the accuracy epsilon for the sound-speed field. The sound speed c_p predicted at a final point by Eq. (30) for an iteration step size of length Δ is compared with the sound speed c_a at the same final point obtained by using the interpolation scheme described in Sections 2.1.2.4 and 2.1.2.5. If $|c_p - c_a|$ is less than ϵ, the program contracts the ray arc increment so that the new ray arc increment Δ' is given by

$$\Delta' = \Delta \frac{\epsilon}{|c_a - c_p|} . \tag{42}$$

Clearly the value given ϵ should depend on the uncertainty in the measurement of the sound-speed field. Typically ϵ is set to 0.5 m/s.

- Δ_{SM} (DELSINMX)—the sine increment test parameter. This parameter examines the effect of the gradients and curvatures of the sound-speed field on a *tentative* iteration of size Δ. If these result in a change in the size of the ray angle greater than Δ_{SM}, the program contracts the iteration step size to Δ', where

$$\Delta' = (\Delta_{SM} / |\sin\theta - \sin\theta_0|)^{1/2}\Delta, \tag{43}$$

in which $\sin\theta_0$ is the sine of the ray angle at an initial point S_0 and $\sin\theta$ is the sine of the ray angle after a tentative iteration of size Δ. To avoid other higher order effects, the iteration interval is first contracted to the lesser of Δ' or

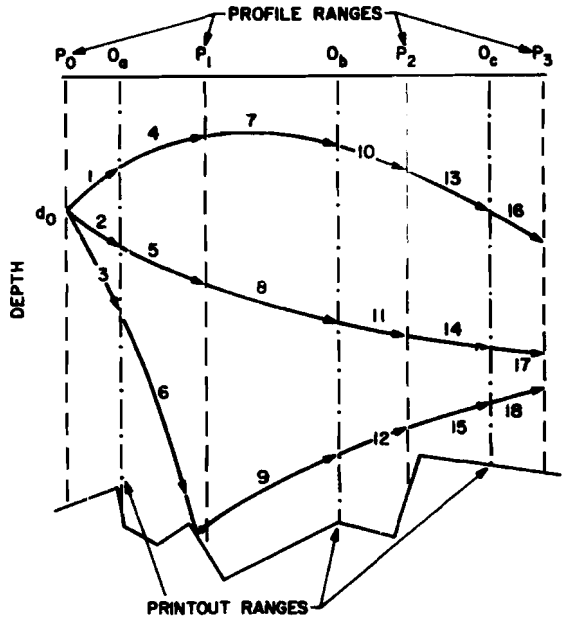

Fig. 12—Order in which SERPENT traces rays in a particular example

$$\Delta'' = (\Delta_{SM} / | w^2 Z(S_0) D(S_0) (\Delta')^3 |)^{1/2} \Delta', \tag{44}$$

where

$$w = \frac{\cos \theta_0}{c(R_0, Z_0)} .$$

Note that equation (III.14b)(ii) of the HLRTP [12k] contains a typographical error and should read as Eq. (44); Δ_{SM} is typically set to 0.02.

3.1.4.3 An Example of the Order of Tracing All Rays Together in Range Segments

The order in which SERPENT traces rays through the sound-speed field differs from the HLRTP and that of most other ray-trace programs. Because of this unique tracing order only two profiles need be resident in core at the same time (hence an unlimited number of profiles can be used), and only one pass need be made through the coefficient tape to trace all the rays, to do all the intensity calculations, to print the ray statistics, and to generate the ray depth distribution plots. This feature also eliminates the need for a time-consuming disk-sort routine (originally used in the HLRTP) to order the rays and plot transmission losses.

Consider the following example illustrated in Fig. 12. Suppose SERPENT is asked to trace three rays through a field having four profiles at ranges P_0, P_1, P_2, and P_3 and also print out the ray statistics and the intensities for some receivers at output ranges O_a, O_b, and O_c. Assume all of the rays start at range P_0 and depth d_0. SERPENT will

begin by tracing the first ray out to range O_a. Then it will trace the second ray to the same range and then the third ray. At this time, since all of the rays are at range O_a, the intensities and ray statistics may be calculated for this output range. Once this output operation is complete, SERPENT will go back to the first ray and trace it to range P_1. Similarly, the second and third rays are traced out to P_1. Now since all of the rays are at P_1, profile P_0 is no longer needed, so it is removed from core and profile P_2 is brought in. This procedure continues as shown until all the rays have reached range P_3, whereupon the output is generated and the program stops.

3.1.4.4 Error Analysis

A detailed error analysis should include considerations of local and global discretion errors, convergence errors, and rounding errors. Underlying all of these is the question of stability [60]. Consideration of these topics is beyond the scope of this report. Some elementary error estimates are however given in the HLRTP [12l].

3.1.5 Theory of Intensity Calculations

3.1.5.1 Describing the Source

The user specifies the source depth, frequency (assumed monochromatic), and beam pattern. SERPENT assumes the source is at range 0 n.mi. Because of the beam pattern, all of the rays will not start with the same initial intensity. In describing the beam pattern the user inputs:

1. The *beam tilt angle*, which is the angle the main beam axis makes with the horizontal (positive angles measured downward).

2. The *axial intensity* I_0 which is the intensity in ergs/s cm^2 along the main beam axis 1 yard from the source. The *axial sound level* is given by

$$A_s = 10 \log_{10} I_0. \tag{45}$$

3. The ratios of the intensities at angles off the main beam axis to the intensity I_0. These beam pattern angles may be nonuniformly spaced and do not have to correspond to the initial ray angles.

The user also specifies the initial ray angles and ray phases θ_k^0 at these angles. That is, all of the rays do not have to begin with the same phase. From this input information SERPENT assigns initial intensities $I_0 f_k$ to each ray k according to its initial angle θ_k^0 at the source ($0 < f_k < 1$). For an omnidirectional beam pattern f_k would be 1 for all of the rays.

3.1.5.2 Random Summation

The phase-independent (Type I random summation in Ref. 12m) *intensity* $I_e(R, z^*)$, for a receiver at range R and depth z^*, may be expressed as a summation over the intensities of the individual rays which arrive at the receiver (arrivals). That is,

$$I_e(R, z^*) = \sum_{k=1}^{N} I_k(R, z^*), \tag{46}$$

where N is the number of arrivals and $I_k(R, z^*)$ is the intensity in ergs/s cm^2 of the kth arrival.

The *measured sound level* at the receiver is defined to be

$$M_{sl} = 10 \log_{10} I_e(R, z^*). \tag{47}$$

The *transmission loss* from the source to the receiver is given by

$$TL(R, z^*) = A_s - M_{sl}. \tag{48}$$

Removing the effect of spherical spreading, we obtain the *transmission anomaly* [61]

$$TA(R, z^*) = TL - 20 \log_{10} (R/r_0), \tag{49}$$

where r_0 is the reference distance. Throughout this report r_0 will be 1 yard.

In traveling from the source to the receiver a ray undergoes a transmission loss L_k, so that

$$I_k(R, z^*) = I_0 f_k \; 10^{-(L_k/10)}. \tag{50}$$

The transmission loss L_k in dB may be expressed as

$$L_k = A'_k + B_k + S_k + G_k, \tag{51}$$

where A'_k is the attenuation loss (neglecting bottom loss), B_k is the loss due to bottom reflections, S_k is the loss due to surface reflections, and G_k is the loss due to geometrical spreading.

The attenuation loss A'_k is assumed to vary linearly with range. That is [58],

$$A'_k = 1000 \, (R - r_0)\alpha, \tag{52}$$

where α is the attenuation coefficient (for refracted-only paths) in dB per kilometer and R and r_0 are measured in meters (Section 2.4).

The bottom loss B_k for the kth arrival is given by

$$B_k = \sum_{i=1}^{n_k} b_{ik}, \tag{53}$$

where n_k is the number of bottom hits experienced by the kth arrival and b_{ik} is the loss due to the ith bottom hit (Section 2.2).

The surface loss S_k for the kth arrival is

$$S_k = \sum_{i=1}^{m_k} s_{ik} = 10\, m_k \log_{10} a, \tag{54}$$

where m_k is the number of surface hits and a is the fractional loss in intensity due to a single surface hit (Section 2.3).

In carrying out our intensity calculations, we assume the medium is cylindrically symmetric. In this approximation the geometrical spreading loss G_k can be shown [62-64] to be

$$G_k = 10 \log_{10}\left(\frac{R}{r_0^2}\frac{\left|\cos\theta_k \left.\frac{\partial z}{\partial \theta_k^0}\right|_R\right|}{\cos\theta_k^0}\right), \tag{55}$$

where θ_k is the angle at which the ray arrives at the receiver (Fig. 13). In Eq. (55), z is the ray depth and the partial derivative is evaluated at the receiver depth. When the partial derivative is zero, G_k approaches negative infinity. When this occurs, we say the ray has touched a *caustic*. In effect the intensity of the ray blows up. Of course ray theory is invalid in the vicinity of a caustic, as mentioned earlier.

Because SERPENT uses a two-dimensional sound-speed field, it, like other similar ray-tracing programs, cannot trace rays directly to the receiver. Instead it traces a group of rays out to the receiver range and then searches the group for those rays which subtend the receiver (Fig. 14).

We will now derive an approximation for Eq. (55) by defining an arrival as two non-terminated rays with indices j and $j+1$ which leave the source at adjacent angles (θ_j^0 and θ_{j+1}^0), subtend the receiver at range R (one ray is deeper than the receiver, and the other is shallower), and have the same number of surface and bottom hits (though they may have a different number of turning points).

To determine the factors in Eq. (55) for the kth arrival, we use the following approximations:

$$\cos\theta_k \approx \cos\theta_j + \frac{(z_j - z^*)}{(z_j - z_{j+1})}(\cos\theta_{j+1} - \cos\theta_j), \tag{56}$$

where

$$\cos\theta_j = (1 - \sin^2\theta_j)^{1/2} \tag{57}$$

and

$$\frac{1}{\cos\theta_k^0}\left|\frac{\partial z}{\partial \theta_k^0}\right|_R\Bigg| \approx \frac{|z_j - z_{j+1}|}{|\sin\theta_j^0 - \sin\theta_{j+1}^0|}. \tag{58}$$

The denominator of Eq. (58) follows from the differential

$$d(\sin\theta) = \cos\theta\, d\theta.$$

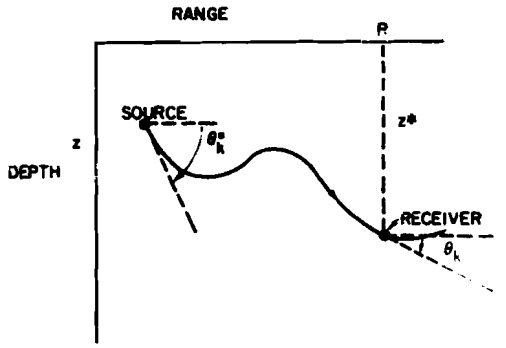

Fig. 13—Ray path from a source to a receiver

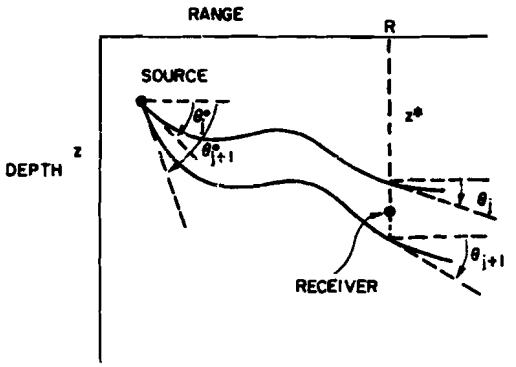

Fig. 14—Two rays subtending a receiver

The effects of surface and bottom loss are included in Eq. (51) by linearly interpolating between the subtending rays. That is,

$$B_k + S_k = 10 \log_{10} Q_k, \tag{59}$$

where

$$Q_k \approx q_j + \frac{z_j - z^*}{z_j - z_{j+1}} (q_{j+1} - q_j),$$

in which

$$q_j = a^{m_j} 10^{-(B_j/10)}, \tag{60}$$

with m_j being the number of surface hits (Eq. (54)).

From the preceding we see we are actually approximating the approximations of ray theory. These approximations become more meaningful as the right-hand side of Eq. (58) approaches the left-hand side. For this to occur, the angular increments between adjacent rays typically have to be very small; as a result an extremely large number of rays have to be traced to achieve meaningful results. As the rays propagate farther and farther

from the source, the number of rays required increases drastically. And, despite the very large number of rays traced, only a very few satisfy the three conditions defining an arrival.

Our experiences with GRASS indicate that though the preceding method of calculating intensities is widely discussed in elementary texts on underwater acoustics, it is not satisfactory for real-world computations. It is expected that more sophisticated procedures will be incorporated into GRASS in the future. (See Section 3.1.7, Recommendations for Improvement.)

3.1.5.3 Coherent Summation

The coherent summation (Type I coherent in Ref. 12m) takes into account the relative phases of the arrivals at the receiver. If the pressure due to each arrival, neglecting the time dependence, has the form

$$P_k \propto I_k^{1/2} e^{i\phi_k}, \tag{61}$$

where I_k is the intensity of the kth arrival and ϕ_k is the phase of the kth arrival, then the resulting Type I coherent intensity at the receiver will be given by

$$I(R,d) \propto \left| \sum_{k=1}^{N_a} P_k \right|^2 = \sum_{k=1}^{N_a} I_k + 2 \sum_{i=1}^{N_a-1} \sum_{j>i}^{N_a} [I_i I_j]^{1/2} \cos(\phi_i - \phi_j). \tag{62}$$

This expression is simply a Type I random summation plus an interference term.

Coherent calculations were initially included in SERPENT to study the Lloyd mirror effect in the case of a simple profile and to check the calculation of travel times. For this purpose they are adequate as described. But for long-range and most short-range real-world problems they are unsatisfactory. As pointed out earlier, SERPENT does not calculate the phases correctly in the vicinity of caustics or correct for phase shifts due to bottom interaction.

3.1.5.4 Statistical Summation

The statistical summation is the Type II intensity calculation described in the HLRTP [12n]. The expression given in that report has been slightly modified, as will be explained.

The Type II intensity is determined as a probability distribution which is obtained by mapping the arrival structure over the ocean depth at a given range. The summation is "pseudo phase independent" and uses *all* the rays that have been traced out to the receiver range, rather than just those which subtend the receiver. Each ray receives a weight in the summation according to its distance from the receiver and other factors. This calculation assumes a "stable" sound-speed field. It is designed primarily for intermediate and long ranges, in contrast to the random/coherent (Type I) calculation, which is mainly for short ranges. Rather than reiterate what has already been said in the HLRTP, we will simply state the expression we use in SERPENT and mention how it differs from that in the HLRTP.

$$I(R, d) = \sum_{i=1}^{N} I_i \epsilon_i \,, \tag{63}$$

where $\epsilon_i = 0$ if the ray was terminated, otherwise $\epsilon_i = 1$. In Eq. (63)

$$I_i = M \frac{r_0^{\,2}}{R} e^{-\alpha R/a} q_i W_i D_i \; D_i^{s} \frac{\chi_i}{2} \frac{\gamma_i^{\,0}}{\gamma_i} \,, \tag{64}$$

where

$$M = \sqrt{\frac{2}{\pi}} \frac{\rho}{\operatorname{erf}\left[\frac{\rho d}{\sqrt{2}}\right] + \operatorname{erf}\left[\frac{\rho(d_B - d)}{\sqrt{2}}\right]} \,, \tag{65}$$

in which $\rho = N^{0.4}/(\sqrt{2}\, d_B)$, $\operatorname{erf}(x) = 2\pi/\sqrt{\pi} \int_0^x e^{-t^2} dt$, and

d_B = the bottom depth

r_0 = reference distance (Eq. (49)),

α = attenuation coefficient (Eq. (52)),

a = a conversion factor for adjusting units,

q_i = factor given by Eq. (60),

N = number of rays traced

W_i = a Gaussian weighting factor = $e^{-2(d_i - d)^2 \rho^2}$,

d_i = the depth of the ith ray,

D_i = receiver directivity function*

$$= 2 \sin^2\left(\frac{2\pi d}{\lambda_{\text{rec}}} \sigma_i\right), \quad \text{if } \frac{d}{\lambda_{\text{rec}}} < 2,$$

$$= 1, \text{ if } \frac{d}{\lambda_{\text{rec}}} \geq 2,$$

in which d is the receiver depth, σ_i is the sine of the ith ray at the receiver, and λ_{rec} is the wavelength at the receiver ($2\pi f/c_{\text{rec}}$), f is the frequency and c_{rec} is the sound speed at the receiver.

*If we assume both up- and down-going rays are traced, the coefficient of the sine given in the HLRTP [12o] should be a 2 rather than 4. A factor of 4 leads to a sharp nonphysical discontinuity at $d/\lambda = 2$. If only down-going rays are traced, the factor 4 is appropriate.

D_i^s = source directivity function

$$= 2 \sin^2\left(\frac{2\pi\, d^s}{\lambda_s}\sigma_i^0\right), \text{ if } \frac{d^s}{\lambda_s} < 2, \tag{68a}$$

$$= 1, \text{ if } \frac{d^s}{\lambda_s} \geqslant 2, \tag{68b}$$

in which d^s is the source depth, σ_i^0 is the sine of the ith ray at the source, λ_s is the wavelength at the source ($2\pi f/c_s$, c_s being the sound speed at the source). SERPENT assumes that $c_{rec} = c_s = 1500$ m/s.

$$\chi_i = \theta_{i+1}^0 - \theta_{i-1}^0, \text{ if } 1 < i < N, \tag{69a}$$

$$\theta_2^0 - \theta_1^0, \text{ if } i = 1, \tag{69b}$$

$$\theta_N^0 - \theta_{N-1}^0, \text{ if } i = N, \tag{69c}$$

γ_i^0 = cosine of the ith ray angle at the source,

γ_i = cosine of the ith ray angle at the receiver

$= \sqrt{1 - \sigma_i^2}$.

The main difference between the calculation just described and that of the HLRTP occurs in the normalization factor M, given by Eq. (65). The coefficient M results from normalizing the Gaussian weights W_i over the depth of the ocean. In performing this normalization the HLRTP [12p] assumed that the bottom was at infinity rather than at the depth d_B. Unfortunately this assumption leads to an error which can become significant when tracing rays through an environment having a widely varying bottom profile.

The Type II summation is called pseudo phase independent because of the terms D_i^s and D_i^r. These terms attempt to account for the Lloyd mirror effect, a phase-dependent phenomena.

3.1.6 Test Methods and Results

3.1.6.1 Untilted and Tilted Hyperbolic-Cosine Profiles

The following is a conceptually straightforward technique for generating range-dependent sound-speed fields having exact ray-path solutions [65]. This technique is useful in that it provides a test for those ray-tracing programs which handle range- and depth-dependent sound-speed fields. The method involves a transformation between two coordinate systems. In one coordinate system the sound-speed field has no depth dependence. In the transformed coordinate system the sound-speed field has both a range and depth dependence. Although this technique could be easily applied to any profile, we will consider only the hyperbolic-cosine profile, which is a degenerate form of the Epstein profile [66, 32a].

(Bucker and Morris [66] discuss the normal-mode solution for the Epstein profile, and Pedersen and Gordon [32a] consider the ray-theory solution.)

Initially two identical profiles were generated by digitizing the expression

$$V = A \cosh B\,(Y - Y_0),$$

where A = 1500 m/s, $B = 3 \times 10^{-4}$ m^{-1}, and Y_0 = 3000 m, at increments of 50 meters from 0 to 6000 meters. These two profiles were inputted in the VFC program, one at 0 and the other at 200 nautical miles, and a coefficient tape was generated. This tape was then fed into PRFPLT. Figure 9 was the result. Next the tape was fed into CTOUR and Fig. 10 resulted. The horizontal lines indicate no horizontal gradients are present. In the unprimed coordinate system of Fig. 15 it is possible to obtain an exact expression for ray depth as a function of range with the source on the channel axis. This expression is illustrated in Fig. 16. The coefficient tape mentioned earlier was fed into SERPENT, and 13 rays (-30° to 30° in 5° steps) were traced through the field for 30 nautical miles. Plotting the resulting ray tape with RATAPE, we obtained Fig. 17. Note the characteristic focusing of the hyperbolic-cosine profile. The symmetry and focusing properties of this profile provide an excellent visual test.

Next, with use of the $X'Y'$ coordinate system of Fig. 15, the expression for the corresponding sound-speed field is shown in Fig. 16. Specific rotation (γ) and translation (b) parameters of 1° and 75 meters respectively were chosen, and 16 profiles were generated from this expression spaced at 2-nautical-mile intervals along the X' axis from 0 to 30 nautical miles. Each such profile had 68 points, and the depths of these points corresponded to the profile depths of the previous example. Figures 18 and 19 show the profiles at 0 and 30 nautical miles. These 16 profiles were entered into the VFC program and another coefficient tape was generated. This tape was fed into CTOUR, and the results are shown in Fig. 20. The slanted lines clearly indicate the presence of a uniform horizontal gradient. Next, 13 rays (-29° to 31° in 5° steps) were traced from a source depth of 2000.3 meters through this sound-speed field. Again characteristic focusing (Fig. 21) was obtained as the rays moved through the field. The exact ray depths versus range can be obtained by applying Newton's method to the corresponding ray-depth expression in Fig. 16.

From comparison of the exact depths against the SERPENT-generated depths for the -30° ray in the XY coordinate system it was found that the difference oscillates with range and has a maximum amplitude of ±5 centimeters over a distance of 30 nautical miles, when Δ_M is set to 125 meters (Section 3.1.4.2).

Likewise comparing the exact depths against the SERPENT-generated depths for the -29° ray in the $X'Y'$ coordinate system (corresponding to the -30° ray in the XY system) a difference was found which oscillates with range and has a maximum amplitude of ±2 meters over the distance of 30 nautical miles. Again for this case we were using Δ_M set to 125 meters.

This test case demonstrates that SERPENT can trace rays through a simple field having a horizontal gradient and yield meaningful results. In testing some other horizontal-gradient ray-tracing programs on this problem, focusing was found to be incomplete owing to an insufficient representation of the sound-speed field.

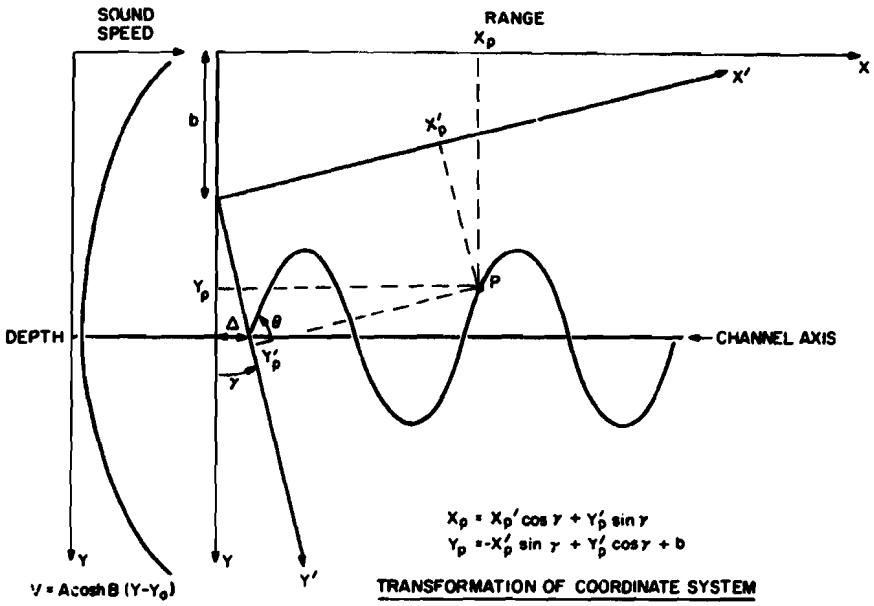

Fig. 15—Transformation of a coordinate system

RAY PATH EQUATIONS FOR HYPERBOLIC COSINE PROFILE WITH SOURCE ON CHANNEL AXIS

IN X-Y COORDINATE SYSTEM:

$$V = \text{SOUND SPEED} = A\cosh B\,(Y - Y_0)$$

$$Y = \text{RAY DEPTH} = Y_0 + \frac{1}{B}\sinh^{-1}\left[\tan\theta \sin B\,(X-\Delta)\right]$$

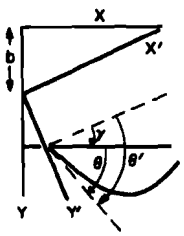

IN X'-Y' COORDINATE SYSTEM:

$$V = \text{SOUND SPEED} = A\cosh B\,(b + Y'c - X'S - Y_0)$$

$$Y' = \text{RAY DEPTH} = TX' - \frac{b}{c} + \frac{1}{c}\left\{Y_0 + \frac{1}{B}\sinh^{-1}\left[\tan(\theta' - \gamma)\sin B\,(X'c + Y'S - \Delta)\right]\right\}$$

WHERE $S = \sin\gamma$

$C = \cos\gamma$

$T = \tan\gamma$

$\Delta = (Y_0 - b)\,T$

Fig. 16—Ray-path equations for a hyperbolic-cosine profile with the source on the channel axis

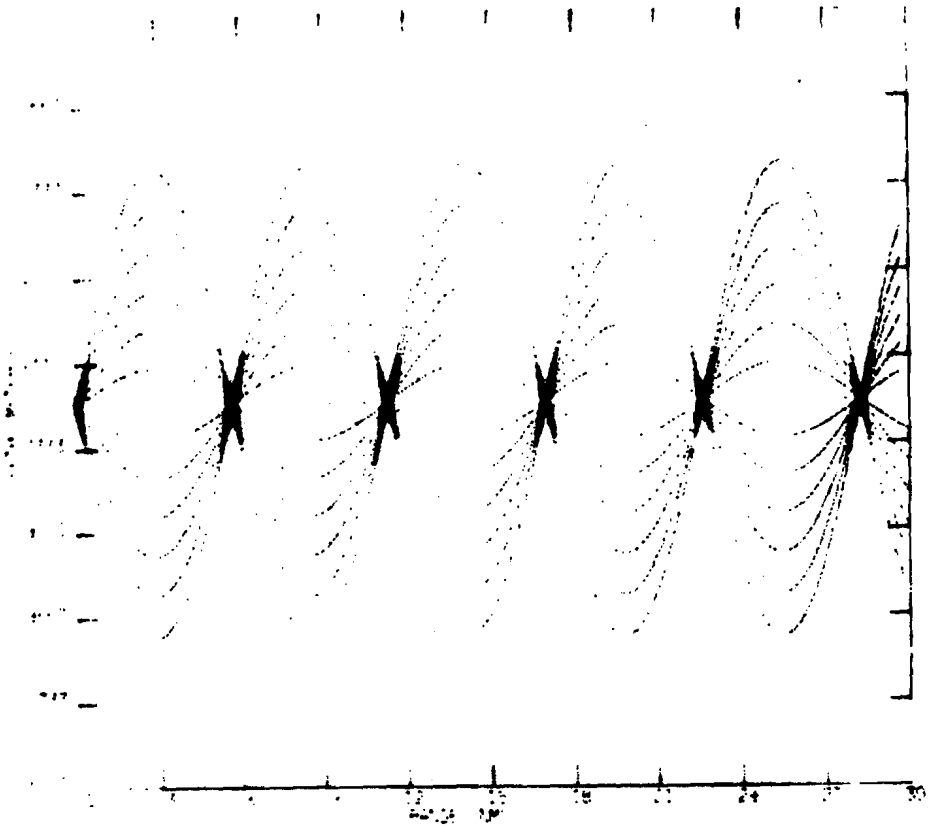

Fig. 17—Ray trace for the hyperbolic-cosine profile

3.1.6.2 Gulf Stream Profiles

A considerably more difficult test case uses the sound-speed field given in Fig. 2 and 3. This field was generated from 16 profiles. A highly variable sound-speed field is clearly evident, especially around 250 nautical miles.

Figure 4 is the ray trace corresponding to this field. A depth transition is made by the rays as they pass through the structure at about 250 nautical miles. This transition could not be predicted by ray-tracing programs which do not provide for horizontal gradients. This figure also serves to illustrate the type of bounding conditions the program can handle.

3.1.7 Recommendations for Improvement

Following are some recommendations for improvement of SIRFERT:

- Iteration equations for individual-ray intensities. As mentioned earlier, SIRFERT does not calculate the intensity of an individual ray as it is being traced. That is, it does not use an iteration equation for intensity. Strong consideration should be given

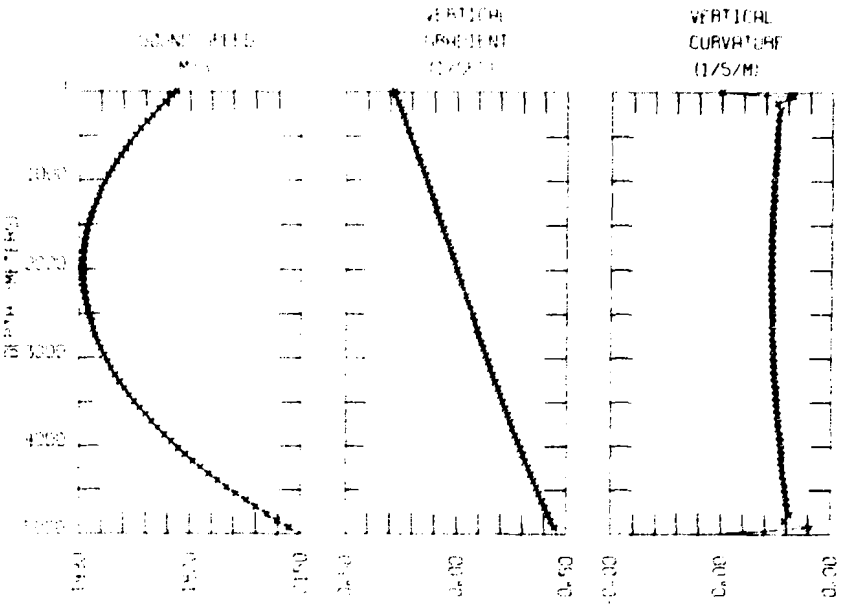

Fig. 18—Tilted hyperbolic-cosine profile at 0 nautical miles. The crosses indicate Taylor series coefficients generated by VFC. The solid lines between points indicate coefficients used in ray tracing.

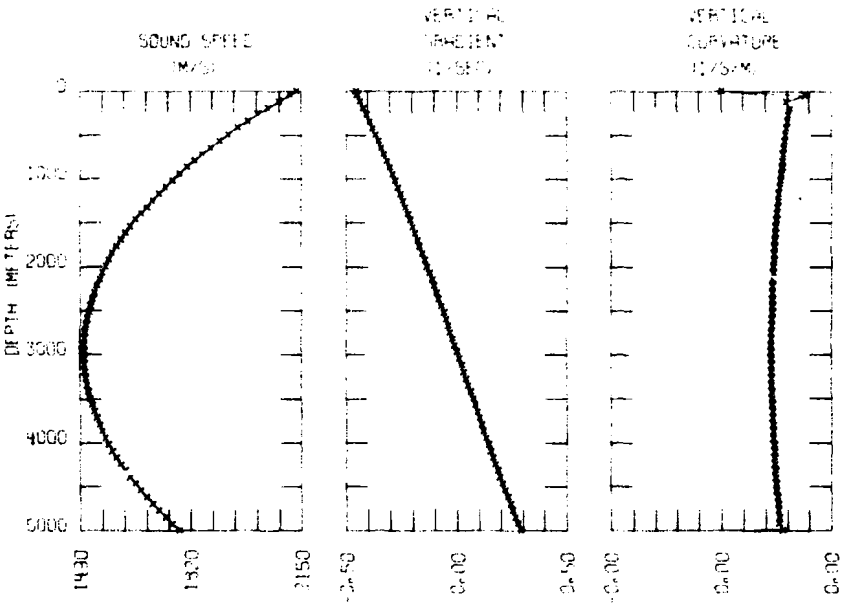

Fig. 19—Tilted hyperbolic-cosine profile at 30 nautical miles

Fig. 20—Contour plot of the filled hyperbolic-cosine sound-speed field

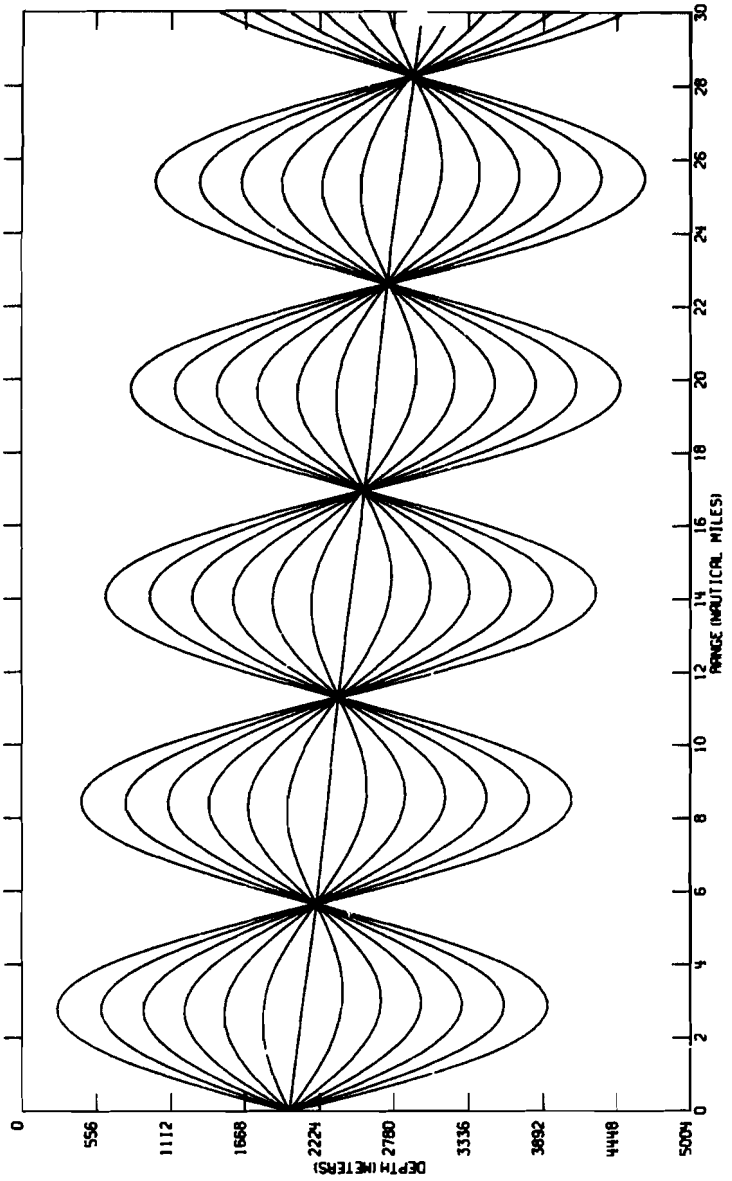

Fig. 21—Ray trace for the tilted hyperbolic-cosine sound-speed field with Δ_M = 125 meters

to incorporating another iteration equation in the program for this purpose. This same recommendation and numerous others were made in the HLRTP [12q] report. Another possibility would be to completely revise the iteration equations, using time as the stepping parameter, rather than ray arc length, as proposed by Wesson [67].

- Calculations at caustics. Along the same lines as the preceding recommendation, consideration should be given to the problem of calculating the correct intensities and phase shifts at caustics. There exists a large body of literature in this area, including Refs. 5, 9, 10, 12r, and 23.

- Optimum step size. The problem of choosing the optimum step size in the iteration equations should be examined further. One approach to this problem might be to consider the iteration equations given in Wesson's paper [67] and then thoroughly examine the numerical-analysis literature for the best approach to solving these equations. Some advantages to this approach are:

  - If the numerical approach is a good one, it is likely that the questions of convergence and stability have already been examined.

  - Other numerical analysts will be aware of the procedure, and it is likely that in the future more light will be shed on these questions.

- Timesharing system. The current version of GRASS was developed using the batch service on a CDC 3800. There would be a number of advantages if further development was carried out in a timesharing environment—preferably with an interactive graphics terminal. The advantages of a timesharing service are discussed in detail in Watson [68]. One earlier objection to the use of timesharing systems was that the ray-tracing programs required too much core. This objection no longer carries much weight because:

  - We have partitioned the "do everything" program into separately executable modules as explained earlier.

  - Current timesharing systems are allowing their user's much more core. For example the CDC Kronos system in Bethesda, Maryland, allows users to have up to 64*K* words of core.

Another drawback of timesharing often cited is the high volume of output required by ray-tracing programs and the slow speed (30 cps) of teletype terminals. This problem can be circumvented by using high-speed (300 cps) line printer terminals such as available on the CDC Export/Import 200 system.

The use of a timesharing system having nationwide coverage would also allow a significantly larger number of scientists to use and participate in the development of the acoustic model without having to implement it on their own machines. The transfer of even well documented Fortran programs from one machine to another can be expensive and frustrating owing to variations in Fortran dialects [21].

3.2 Generating Ray Diagrams (RAPLOT Program)

3.2.1 Purpose

The purpose of RAPLOT is to generate accurate Calcomp ray plots showing the bottom-profile.

3.2.2 Input

The input to RAPLOT consists of:

- The ray tape generated by SERPENT.
- Control parameters on cards which select the number of plots to be generated, the rays to be displayed on each plot, the plot sizes, scaling parameters, and the graph titles to be displayed on each figure.

3.2.3 Output

The output consists of:

- Labeled Calcomp plots showing the rays and the bottom profile (Figs. 4, 17, and 21).
- A printer listing of the input and control parameters.

3.2.4 Recommendation for Improvement

The utility of the ray diagrams could be increased by adding timing information to them. Since the ray-statistics tape already contains timing information, this would be a straightforward programming task. An example of how this information would appear on a ray diagram is given in Fig. 1 of Ref. 16.

3.3 Generating Transmission-Loss Plots (LOSSPLT Program)

3.3.1 Purpose

The purpose of LOSSPLT is to generate Calcomp plots of transmission-loss versus range.

3.3.2 Input

The input consists of:

- Transmission-loss tape generated by SERPENT.
- Control parameters and graph titles on cards.

3.3.3 Output

The output consists of:

- Labeled Calcomp plots of transmission loss versus range. If requested, these plots will display random loss (Type I), coherent loss (Type I), and statistical (Type II) transmission loss together with user input experimental data or theoretical curves for comparison.

- A printer listing of transmission-loss values and control parameters.

4. CONCLUSIONS AND RECOMMENDATIONS

The current version of GRASS should be considered as an initial step in the development of a comprehensive model of long-range acoustic propagation in the deep ocean. Theoretically and functionally the system is very similar to the Hudson Laboratories ray-tracing program.

The main features of the system are described in Section 1.2. Currently, the system yields very good ray-path results for complicated bathymetries, but it is not yet state of the art in terms of intensity calculations. There is however a large body of literature pointing to directions in which the system could be developed. Some recommendations are given in Sections 2.1.1.5, 2.1.2.9, 2.1.4.6, 3.1.7, and 3.2.4.

REFERENCES

1. L. Camp, *Underwater Acoustics*, Wiley-Interscience, New York, 1970, pp. 50-56.
2. A.V. Newman and F. Ingenito, "A Normal Mode Computer Program for Calculating Sound Propagation in Shallow Water With an Arbitrary Velocity Profile," NRL Memorandum Report 2381, Jan. 1972.
3. J.W. Caruthers, "Lecture Notes on Marine Acoustics," Texas A&MU Sea Grant Publication TAMU-SG-71-403, June 1968, Vol. I, p. 130.
4. A.O. Williams, Jr., "Normal Modes in Propagation of Underwater Sound," Chapter 2 in *Underwater Acoustics*, R.W.B. Stephens, editor, Wiley-Interscience, London, New York, 1970, p. 30.
5. C.W. Spofford, "The Future of Long Range Transmission Loss Predictions," Bell Telephone Laboratories, Inc., Whippany, New Jersey, July, 1971.
6. H.W. Marsh, Jr., "The Use of Ray Methods and First Order Diffraction Corrections," U.S. Navy Underwater Sound Laboratory Tech. Memo. 1100-61-54, Sept. 1954.
7. J.B. Keller, "A Geometrical Theory of Diffraction," Proc. Symposia in Applied Mathematics Proceedings, McGraw-Hill, New York, 1958, Vol. 8, pp. 27-52.
8. R.N. Buchal and J.B. Keller, "Boundary Layer Problems in Diffraction Theory," Comm. Pure App. Math. 13, 85-114 (1960).
9. D. Ludwig, "Uniform Asymptotic Expansions at a Caustic," Comm. Pure App. Math. 19, 215-250 (1966).

10. Y.A. Kravtsov, "Asymptotic Solutions of Maxwell's Equations Near a Caustic," Radiofizika 7, 1049-1056 (1964), Bell Telephone Laboratories translation.

11. L.P. Solomon, "Geometrical Acoustic Propagation With Frequency Dependence," J. Acoust. Soc. Am. 44, 1115-1120 (1968).

12. H. Davis, H. Fleming, W.A. Hardy, R. Miningham, S. Rosenbaum, "The Hudson Laboratories Ray Tracing Program," Hudson Laboratories, Columbia University, Technical Report 150, June 1968:

(a) pp. 7-9	(g) pp. 5, 6	(m) p. 95
(b) pp. 1-363	(h) pp. 55-59	(n) pp. 96-99
(c) pp. 5, 88, 89	(i) p. 215	(o) p. 86
(d) pp. 1, 7	(j) pp. 59-66	(p) p. 97, Eq. (IV.45)
(e) pp. 49, 51	(k) p. 61	(q) pp. 308-320
(f) pp. 69-73	(l) pp. 64-66	(r) pp. 323-349.

13. M.A. Pedersen and D.F. Gordon, Theoretical Investigation of a Double Family of Normal Modes in an Underwater Acoustic Surface Duct," J. Acoust. Soc. Am. 47, 304-326 (1970).

14. K.G. Budden. *The Wave-Guide Mode Theory of Wave Propagation*, Logos Press, London, and Prentice-Hall, Englewood Cliffs, N.J., 1961.

15. D.E. Kerr, editor, *Propagation of Short Radio Waves*, McGraw-Hill, New York, 1951, p. 65.

16. J.M. Kelso, "Ray Tracing in the Ionosphere," Radio Science 3, 1-12 (1968).

17. A.J.W. Sommerfeld, *Optics*, Academic Press, New York, 1954, pp. 207, 337.

18. M. Klerer and J. May, "A User Oriented Programming Language," Computer J. 8, 103 (1965).

19. M. Klerer and J. May, "Two Dimensional Programming," Fall Joint Computer Conference, AFIPS 27, 63 (1965).

20. M. Klerer and J. May, "Algorithms for Analysis and Translation of a Special Set of Computable Mathematical Forms," Hudson Laboratories, Columbia University, Technical Report 113, 1963.

21. R.L. Berkowitz, "A Comparison of Some Fortran Languages," NRL Memorandum Report 2191, Oct. 1970.

22. F.C. Fuglister, *Atlantic Ocean Atlas of Temperature and Salinity Profiles*, Woods Hole Oceanographic Institution, Woods Hole, Mass., 1960.

23. P. Ugincius, "Intensity Equations in Ray Acoustics, I," J. Acoust. Soc. Am. 45, 193 (1969).

24. S.R. Murphy and G.E. Lord, "Thermal and Sound Velocity Microstructure Data Taken with an Unmanned Research Vehicle," Univ. of Wash. Applied Physics Lab. Report 6523, 1965.

25. E.R. Anderson, "Distribution of Sound Velocity in a Section of the Eastern North Pacific," Trans. Am. Geophys. Union 31, 221-228 (1950).

26. J.T. Warfield and M.J. Jacobson, "Acoustic Propagation in a Channel With Range-Dependent Sound Speed," J. Acoust. Soc. Am. 45, 1145 (1969).

27. D.M. Milder, "Ray and Wave Invariants for SOFAR Channel Propagation," J. Acoust. Soc. Am. 46, 1259-1263 (1969).

28. E.L. Wright, "Ray Tracing With Horizontal and Vertical Gradients" (TRIMAIN), Paper N8, 79th Meeting of the Acoust. Soc. of Am., 21-24 Apr. 1970, Atlantic City.

29. P. Wolff, ONR Liason Officer for Acoustic Fleet Numerical Weather Central, Monterey, California. C.W. Spofford, Maury Center, NRL, Washington, D.C.

30. M.A. Pedersen, "Acoustic Intensity Anomalies Introduced by Constant Velocity Gradients," J. Acoust. Soc. Am. 33, 465-474 (1961).

31. H. Weinberg, "A Continuous-Gradient Curve-Fitting Technique for Acoustic-Ray Analysis," J. Acoust. Soc. Am. 50, 975 (1971):
    (a) p. 984 (b) p. 979 (c) p. 975 (d) p. 980.

32. M.A. Pedersen and D.F. Gordon, "Comparison of Curvilinear and Linear Profile Approximation in the Calculation of Underwater Sound Intensities by Ray Theory," J. Acoust. Soc. Am. 41, 419-438 (1967):
    (a) pp. 424, 425.

33. M.A. Pedersen, "Ray Theory Applied to a Wide Class of Velocity Functions," J. Acoust. Soc. Am. 43, 619-634 (1968).

34. M.K. Miller, "Calculation of Horizontal Ranges and Sound Intensities by Use of Numerical Integration Techniques," J. Acoust. Soc. Am. 44, 1690-1698 (1968).

35. C.C. Leroy, "Development of Simple Equations for Accurate and More Realistic Calculation of the Speed of Sound in Seawater," J. Acoust. Soc. Am. 46, 216-226 (1969).

36. C.C. Leroy, "Formulas for the Calculation of Underwater Pressure in Acoustics," J. Acoust. Soc. Am. 44, 651-653 (1968).

37. A. Hassitt, "Design and Implementation of a General-Purpose Input Routine," Comm. ACM 7, 350 (1964).

38. W.D. Wilson, "Equation for the Speed of Sound in Sea Water," J. Acoust. Soc. Am. 32, 1357 (1960).

39. A. Skretting, "Sound Field Computation by Means of Desk Top Computers," SACLANT ASW Research Center, Technical Report 141, 15 Mar. 1969 (NATO Unclassified).

40. H.W. Frye and J.D. Pugh, "A New Equation for the Speed of Sound in Seawater," J. Acoust. Soc. Am. 50, 384 (1971).

41. M. Rattray, Jr., "Interpolation Errors and Oceanographic Sampling," Deep Sea Res. 9, 25-37 (1962).

42. T.N.E. Greville, "Spline Functions, Interpolation, and Numerical Quadrature," pp. 156-168 in *Mathematical Methods for Digital Computers*, Vol. II, A. Ralston and H.S. Wilf, editors, Wiley, New York, 1967.

43. S.D. Conte and C. deBoor, *Elementary Numerical Analysis: An Algorithmic Approach*, 2nd edition, McGraw-Hill, New York, 1972, pp. 231-240.

44. J.H. Ahlberg, E.N. Nilson, and J.L. Walsh, *The Theory of Splines and Their Applications*, Academic Press, New York, 1967.

45. G. Birkhoff and H.L. Garabedian, "Smooth Surface Interpolation," J. Math. and Physics 39, 258-268 (1960).

46. M.J.D. Powell, "Curve Fitting by Splines in One Variable," pp. 65-83 in *Numerical Approximation to Functions and Data*, J.G. Hayes, editor, Oxford Univ. Press, New York, 1970.

47. C.B. Moler and L.P. Solomon, "Use of Splines and Numerical Integration in Geometrical Acoustics," J. Acoust. Soc. Am. 48, 739-744 (1970).

48. M.R. Spiegel, *Schaum's Outline of Theory and Problems of Complex Variables*, Schaum, New York, 1964, pp. 200, 201.

49. A.G.D. Watson, "The Effect of the Earth's Sphericity on the Propagation of Sound in the Sea," Great Britain Admiralty Res. Lab. Report ARL/N29/L, Dec. 1958.

50. N. Bowditch, *American Practical Navigator*, Navy Hydrographic Office Publication 9, Government Printing Office, 1962, p. 957.

51. J.J. Cornyn, "Fortran Subroutines for Bicubic Spline Interpolation," NRL Memorandum Report 2596 (Computer Bulletin 32), June 1973. AD-762419.

52. C. deBoor, "Bicubic Spline Interpolation," J. Math. and Physics 41, 212-218 (1962).

53. J.B. Rosen, "Minimum Error Bounds for Multidimensional Spline Approximation," J. Computer and System Sciences 5, 430-452 (1971).

54. F.D. Clarke and L.V. Blake, "Fortran Subroutines for Conversion of Calcomp Plot Programs to Gerber-Plotter Magnetic-Tape Output," NRL Memorandum Report 2377 (NRL Computer Bulletin 26), Dec. 1971.

55. E.E. Branstetter, "CONTOUR, A Fortran Subroutine for Producing Contour Maps," Oak Ridge National Laboratory Report ORNL-4031, Nov. 1966.

56. H.A. Brown, "A CDC 3800 Computer Subroutine for Producing Isometric Plots on the 565 Calcomp Plotter," NRL Computer Notes 31 (1969) and 31A (1970).

57. H. Williamson, "Algorithm 420—Hidden-Line Plotting Program [J6]," Comm. ACM 15, 100-103 (1972).

58. W.H. Thorp, "Deep-Ocean Sound Attenuation in the Sub- and Low-Kilocycle-per-Second Region," J. Acoust. Soc. Am. 38, 648-654 (1965).

59. L. Montagnino, "Ray Tracing in Inhomogeneous Media," J. Opt. Soc. Am. 58, 1667 (1968).

60. J.M. Ortega, *Numerical Analysis (A Second Course)*, Academic Press, New York, 1972, pp. 1-4.

61. *Principles and Applications of Underwater Sound*, Naval Material Command, NAVMAT P-9674, 1968, pp. 8, 9.

62. C.B. Officer, *Introduction to the Theory of Sound Transmission, With Application to the Ocean*, McGraw-Hill, New York, 1958.

63. E.S. Eby and L.T. Einstein, "General Spreading-Loss Expression," J. Acoust. Soc. Am. 52, 455 (1972); 37, 933-934(L) (1965).

64. I. Tolstoy and C.S. Clay, *Ocean Acoustics*, McGraw-Hill, New York, 1966.

65. J.J. Cornyn, "Technique for the Generation of Range Dependent Sound-Velocity Fields," J. Acoust. Soc. Am. 48, 92(A) (1970).

66. H.P. Bucker and H.E. Morris, "Epstein Normal-Mode Model of a Surface Duct," J. Acoust. Soc. Am. 41, 1475-1478 (1967).

67. R.L. Wesson, "A Time Integration Method for Computation of the Intensities of Seismic Rays," Bull. Seism. Soc. Am. 60, 307-316 (1970).

68. R.W. Watson, *Timesharing System Design Concepts*, McGraw-Hill, New York, 1970, Chapter 1.

APPENDIX

Basic Ray-Acoustics Theory

Starting with Eq. (1), we assume that Φ may be expressed as

$$\Phi = \phi(\bar{r})e^{i\omega t}, \tag{A1}$$

where $\bar{r}$ is the spatial coordinate and ω is the angular frequency.

Using the relation

$$k = \frac{2\pi}{\lambda} = \frac{\omega}{c} \tag{A2}$$

between the wavenumber k, the angular frequency ω, and the sound-speed c, and substituting the derivatives of Φ into Eq. (1), we obtain the time-independent scalar wave equation

$$\nabla^2\phi + k^2\phi = 0. \tag{A3}$$

We see that as $\lambda \rightarrow 0$ this equation degenerates. To obtain a quantitative conclusion from the above equation, we assume

$$\phi(\bar{r}) = A\, e^{ik_0 \mathcal{S}} \tag{A4}$$

where $A(\bar{r}) = A(x, R, z)$ is an amplitude factor and $\mathcal{S} = \mathcal{S}\ (x, R, z)$ is the eikonal (eikon being the Greek word for image).

This assumption takes us into the realm of ray theory as opposed to wave theory. Wave theory attempts to solve Eq. (A3) for ϕ assuming a particular set of source and boundary conditions. Ray theory, on the other hand, assumes a particular form for Φ and then substitutes this form into the wave equation to derive another differential equation which is more amenable to solution. This new equation is referred to as the eikonal equation.

We note that k_0 may approach infinity in Eq. (A4), so ϕ may be a rapidly varying function of position while A and $\mathcal{S}$ are slowly varying functions which do not go to infinity with k_0. Differentiating Eq. (A4) and substituting the result into Eq. (A3), we obtain

$$A(\eta^2 - |\nabla \mathcal{S}|^2) + \frac{\nabla^2 A}{k_0^2} + \frac{i}{k_0}(A\nabla^2\mathcal{S} + 2\nabla A \cdot \nabla \mathcal{S}) = 0,$$

where η is the spatially dependent index of refraction

$$\eta \equiv \frac{c_0}{c} = \frac{k}{k_0}. \tag{A6}$$

Of course the real and imaginary terms of Eq. (A5) must vanish independently. Noting that A cannot be zero everywhere, and making the crucial assumptions [A1]

$$\nabla^2 A \ll k_0^2 \tag{A7}$$

and

$$A\nabla\delta^2 \quad + 2\nabla A \cdot \nabla\delta \ll k_0, \tag{A8}$$

we obtain

$$|\nabla\delta|^2 = \eta^2. \tag{A9}$$

Equation (A9), a first-order partial differential equation, is the eikonal equation mentioned earlier and represents one of several equivalent formulations of geometrical acoustics. Some of the other formulations include Snell's law, the Hamilton-Jacobi equation, and Fermat's principle [A2].

The condition given as Eq. (A7) is violated in any region containing localized sources. In addition significant changes in amplitude may occur as the result of diffraction effects in the vicinity of a shadow boundary, at the edges of obstacles, at a caustic, or at a focal point. As a consequence ∇A may be large and the second condition, Eq. (A8), may be violated. Further it can be shown [A3] that that validity of Eq. (A9) requires

$$\left|\frac{\nabla\eta}{\eta}\right| \ll k. \tag{A10}$$

That is, the fractional change in the index of refraction over the distance of a wavelength must be very small compared to unity. Clearly this condition will not be met at the ocean's surface and bottom or in regions where the sound speed changes significantly over the distance of a wavelength. Diffraction effects are still possible around the edges of obstacles even though they may be located in regions of a smoothly varying index of refraction.

Another condition under which the eikonal equation is not a good approximate solution of the wave equation occurs when the wavefront curvature is large, or, in terms of rays (a concept defined below), when the radius of curvature of a ray is the order of or smaller than a wavelength.

Once Eq. (A9) has been integrated to obtain δ, Eq. (A8) gives the component of $\nabla A/A$ in the direction of $\nabla\delta$. No statement is made about the component of $\nabla A/A$ perpendicular to $\nabla\delta$. Hence these components can be discontinuous.

The solutions δ to the eikonal equation are surfaces of constant phase, or wavefronts. The orthogonal trajectories of these surfaces are defined to be *rays*. Hence the direction of the acoustic rays is given by a unit vector normal to the eikonal surface and passing through the point in question:

$$\hat{s} = \frac{\nabla S}{|\nabla S|} = \frac{\nabla S}{\eta}. \tag{A11}$$

This unit vector is frequently referred to as the *ray vector*. Since $\nabla \times \nabla S = 0$, it follows that

$$\nabla \times (\eta \hat{s}) = 0. \tag{A12}$$

This condition is equivalent to the existence of the eikonal [A4].

The *ray curvature K* is defined to be

$$\overline{K} \equiv \frac{d\hat{s}}{ds}, \tag{A13}$$

where $d\hat{s}$ is a change in the ray vector and ds is an increment in ray arc length. Since

$$\frac{d\hat{s}}{ds} = \frac{\partial \hat{s}}{\partial x}\frac{dx}{ds} + \frac{\partial \hat{s}}{\partial R}\frac{dR}{ds} + \frac{\partial \hat{s}}{\partial z}\frac{dz}{ds} \tag{A14}$$

and since $dx/ds, \ldots$ is the $x, \ldots$ component of the unit vector $\hat{s}$, we have (letting $s_x = dx/ds$, etc.)

$$\frac{d\hat{s}}{ds} = \frac{\partial \hat{s}}{\partial x} s_x + \frac{\partial \hat{s}}{\partial R} s_R + \frac{\partial \hat{s}}{\partial z} s_z \tag{A15}$$

or

$$\overline{K} = \frac{d\hat{s}}{ds} = (\hat{s}\cdot\nabla)\hat{s}. \tag{A16}$$

For any two vectors $\overline{F}$ and $\overline{G}$ the following identity holds:

$$\nabla(\overline{F}\cdot\overline{G}) = \overline{F} \times (\nabla \times \overline{G}) + \overline{G} \times (\nabla \times \overline{F}) + (\overline{F}\cdot\nabla)\overline{G} + (\overline{G}\cdot\nabla)\overline{F}. \tag{A17}$$

Using this relationship and replacing $\overline{F}$ and $\overline{G}$ with the unit vector $\hat{s}$ and noting $\hat{s}\cdot\hat{s} = 1$, we have

$$\nabla(\hat{s}\cdot\hat{s}) = 2[\hat{s} \times (\nabla \times \hat{s}) + \overline{K}] = 0 \tag{A18}$$

or

$$\overline{K} = (\nabla \times \hat{s}) \times \hat{s}.$$

Returning to Eq. (A12) and rewriting it as

$$\nabla \times \hat{s} = \frac{1}{\eta}[\hat{s} \times \nabla\eta] \tag{A19}$$

and substituting this expression into Eq. (A18), we have

$$\bar{K} = \frac{1}{\eta}[\hat{s} \times \nabla\eta] \times \hat{s}.$$

Since for any three vectors $\bar{A}$, $\bar{B}$, and $\bar{C}$,

$$(\bar{A} \times \bar{B}) \times \bar{C} = \bar{B}(\bar{A}\cdot\bar{C}) - \bar{A}(\bar{B}\cdot\bar{C}),$$

it follows that

$$\bar{K} = \frac{1}{\eta}[\nabla\eta - \hat{s}(\nabla\eta\cdot\hat{s})]. \tag{A20}$$

From this equation we see that $\bar{K}$, $\nabla\eta$, and $\hat{s}$ all lie on the same plane. We also see that if the medium is homogeneous, $\nabla\eta$ and thus $\bar{K}$ will be 0 and the rays will move in straight lines.

REFERENCES

A1. J.M. Kelso, "Ray Tracing in the Ionosphere," Radio Science 3, 1-12 (1968), p. 3.

A2. H. Goldstein, *Classical Mechanics*, Addison-Wesley, Cambridge, Mass., 1959, 7th edition, pp. 307-314.

A3. J.M. Pearson, *A Theory of Waves*, Allyn and Bacon, Boston, 1966, p. 120.

A4. A. Sommerfeld, *Optics*, Academic Press, New York, 1954, p. 337.

☆U.S. GOVERNMENT PRINTING OFFICE: 1974 542-170/221 1-3